Shared and differential features of Robo3 expression pattern in amniotes

François Friocourt, Peter Kozulin, Morgane Belle, Rodrigo J Suárez, Nicolas Di-Poï, Linda J Richards, Paolo Giacobini, Alain Chédotal

Shared and differential features of Robo3 expression pattern in amniotes

François Friocourt[1], Peter Kozulin[2], Morgane Belle[1], Rodrigo Suárez[2], Nicolas Di-Poï[3], Linda J. Richards[2, 4], Paolo Giacobini[5, 6, 7] and Alain Chédotal[1, 8]

[1]Sorbonne Université, INSERM, CNRS, Institut de la Vision, 17 Rue Moreau, F-75012 Paris, France.

[2]The Queensland Brain Institute, The University of Queensland, Brisbane, Queensland, Australia.

[3]Research Program in Developmental Biology, Institute of Biotechnology, University of Helsinki, 00014 Helsinki, Finland

[4]The School of Biomedical Sciences, The University of Queensland, Brisbane, Queensland, Australia.

[5]University of Lille, UMR-S 1172 - JPArc - Centre de Recherche Jean-Pierre AUBERT Neurosciences et Cancer, Lille 59000, France.

[6]Inserm, UMR-S 1172, Laboratory of Development and Plasticity of the Neuroendocrine Brain, Lille 59000, France.

[7]FHU 1,000 Days for Health, University of Lille, School of Medicine, Lille 5900, France

[8]Corresponding author : alain.chedotal@inserm.fr

Running title: Robo3 expression in developing amniotes

ACKNOWLEDGEMENTS

This work was supported by grants from the Agence Nationale de la Recherche (ANR) (ANR-14-CE13-0004-01) (AC). It was performed in the frame of the LABEX LIFESENSES (reference ANR-10-LABX-65) supported by French state funds managed by the ANR within the Investissements d'Avenir programme under reference ANR-11-IDEX-0004-02 (AC). Marsupial work was supported by the Australian Research Council (DP160103958 to L.J.R. and R.S., and DE160101394 to R.S.), the National Health and Medical Research Council (GNT1120615 to L.J.R., and GNT1035093 to PK) with animals bred by the University of Queensland Biological Resources and Native Wildlife Teaching and Research Facility. We thank Sergi Roig Puiggros for helping with *in situ* hybridization experiments.

ABSTRACT

In Bilaterians, commissural neurons project their axons across the midline of the nervous system to target neurons on the opposite side. In mammals, midline crossing at the level of the hindbrain and spinal cord requires the Robo3 receptor which is transiently expressed by all commissural neurons. Unlike other Robo receptors, mammalian Robo3 receptors do not bind Slit ligands and promote midline crossing. Surprisingly, not much is known about Robo3 distribution and mechanism of action in other vertebrate species.

Here, we have use whole-mount immunostaining, tissue clearing and light-sheet fluorescent microscopy to study Robo3 expression pattern in multiple embryonic tissue from diverse representatives of amniotes at distinct stages, including squamate (African house snake), birds (chicken, duck, pigeon, ostrich, emu and zebra finch), early postnatal marsupial mammals (fat-tailed dunnart), and eutherian mammals (mouse and human). The analysis of this rich and unique repertoire of amniote specimen reveals conserved features of Robo3 expression in midbrain, hindbrain and spinal cord commissural circuits, which together with subtle but meaningful modifications could account for species-specific evolution of sensory-motor and cognitive capacities. Our results also highlight important differences of precerebellar nuclei development across amniotes.

KEYWORDS

Robo3, commissures, amniotes, development, evolution, inferior olive, pontine nucleus, habenula, RRID: AB_2181865, RRID: AB_2107107, RRID: AB_2107124, RRID: AB_1078266, RRID: AB_2315065, RRID: AB_881306, RRID: AB_2313773,

RRID: AB_262133, RRID: AB_2732861, RRID: AB_2340880, RRID: AB_2340885, RRID: AB_2307443, RRID: AB_2492288, RRID: AB_2651135, RRID: SCR_007370.

INTRODUCTION

Bilateral coordination in the nervous system is essential for cognitive, sensory and motor integration in vertebrates irrespective of whether they walk, swim, fly or crawl (Brown et al., 1999; Goulding, 2009). This coordination is achieved by axonal connections that link the left and right central nervous system, called commissures. Commissural wiring is a highly controlled developmental process, and deficits in commissural development have been associated with multiple syndromes in humans, ranging from minor motor deficits, like horizontal gaze palsy or mirror movements, to severe sensory-motor and cognitive deficits (Paul et al., 2007; Welniarz et al., 2015; Jamuar et al., 2017). Commissural connections incorporate multiple and diverse central nervous (CNS) systems, some of which are specific to vertebrate subgroups (Suárez et al., 2014). For example, the cortico-spinal tract that connects the motor cortex to contralateral spinal cord motor neurons is only present in mammals (Welniarz et al., 2017). Likewise, the major telencephalic commissural tract in human, the corpus callosum, is only found in eutherian mammals, but not in marsupials or monotremes, and diprotodont marsupials evolved a new commissural route through the internal capsule (Aboitiz and Montiel, 2003). As commissural circuits have undergone several modifications in a lineage-specific manner during vertebrate evolution, comparisons of homologous traits are not always easy to establish. For example, retinal ganglion cell projections to the brain are partially uncrossed in mammals and amphibians, as opposed to the fully crossed optic chiasm found in adult birds and most fish (Petros et al., 2008; Martin, 2009).

Similarly, birds differ from other vertebrates in the origins and proportions of axons connecting both telencephalic hemispheres (Letzner et al., 2016; Paterson and Bottjer, 2017), and similar circuits between cortical hemispheres are present in mammals despite the route taken by commissural axons (Suárez et al., 2018). Furthermore, spinal cord commissural circuits organization have undergone extensive variation associated with the evolution of different locomotion strategies in vertebrates (Kiehn, 2016). Therefore, adaptations in commissural circuits might account for the emergence of new abilities including binocular vision, interhemispheric transfer, tetrapedal locomotion and/or flight.

Commissural circuit diversification in vertebrates is likely to arise from axon guidance adaptations during development (Petros et al., 2008; Suárez et al., 2014). The Robo3 transmembrane receptor belongs to the Roundabout (Robo) family of transmembrane receptors and plays a key role in commissural axon guidance (Chédotal, 2011; Friocourt and Chédotal, 2017). In mice, Robo3 is transiently expressed in most commissural tracts in the midbrain, hindbrain and spinal cord (Belle et al., 2014; Zelina et al., 2014). Nonetheless, Robo3 is also found in some non-commissural neurons, including migrating cortical interneurons (Barber et al., 2009). In mammals, Robo3 expression has only been studied in mice, but it was also detected in human pontine neurons (Jen et al., 2004). Regarding other amniotes, Robo3 expression has been reported in birds at spinal cord and hindbrain commissural axons during early developmental stages (Philipp et al., 2012; Escalante et al., 2013; Friocourt et al., 2017). However, no extensive comparative expression data is available in this vertebrate clade, especially at later developmental stages. Similarly, Robo3 expression patterns in fish and amphibians are poorly described, but at least include ipsilaterally projecting neurons in zebrafish (Challa et

al., 2001; Hocking et al., 2010; Schweitzer et al., 2013). Therefore, different patterns of Robo3 expression in vertebrates might correlate with recent findings concerning modifications of Robo3 function in mammals (Zelina et al., 2014).

Here, we took advantage of recent advances in three-dimension (3D) imaging techniques, associating *in toto* immunostaining and tissue clearing, to study Robo3 expression during vertebrate early brain development.

METHODS

Animals

All procedures were performed in accordance to the guidelines approved by French Ministry of Agriculture and Sorbonne Université ethic committee.

Mouse embryos (*Mus musculus RjOrl:SWISS*) were collected from pregnant females provided by Janviers Labs (Le Genest-Saint-Isle – France). The day of vaginal plug is considered as Embryonic day 0 (E0). Brains were dissected for stages described in Table S1.

Fat tailed dunnart joeys (*Sminthopsis crassicaudata*) were obtained from a breeding colony at the Native Wildlife Teaching and Research Facility, The University of Queensland. All animal procedures, including laboratory breeding, were approved by The University of Queensland Animal Ethics Committee and the Queensland Government Department of Environment and Heritage Protection, and were performed according to the current Australian Code for the Care and Use of Animals for Scientific Purposes (NHMRC, 8th edition, 2013), as well as international guidelines on animal welfare. Pouches were checked every second day for joeys, and day of young detection was recorded and animals were staged as previously reported (Suárez et al., 2017). Individual joeys were collected at different postnatal

stages as previously reported (Paolino et al., 2018)(see Table S1). The skin over the scalp was removed from postnatal day 2 (P2) and P4 prior to immunostaining, to enable optimal antibody penetration. For later stages, brains were dissected before processing.

African house snake embryos (*Boaedon fuliginosus*) were collected from a breeding colony at University of Helsinki, Helsinki – Finland, as previously described (Di-Poï and Milinkovitch, 2016). Fertilized eggs were incubated on a moistened vermiculite substrate at 29.5°C. Embryos were removed at different embryonic days post-oviposition (dpo) and staged on the basis of their external morphology according to complete developmental tables available for this snake species (Boback et al., 2012). Duck embryos (*Anas platyrhynchos*) were kindly provided by Clémence Kress and Bertrand Pain from Université Lyon I, Lyon - France. Zebra finch (*Taeniopygia guttata*) and Emu (*Dromaius novaehollandiae*) embryos were kindly provided by Magdalena Hidalgo, Nicolas Haupaix and Marie Manceau from Collège de France, Paris - France. Pigeon (Columba livia), Chicken (*Gallus gallus*), Ostrich (*Struthio camelus*) embryos were directly collected and processed by FF. All bird eggs were incubated at 37°C in humid conditions. Embryos were collected at different time points depending on their embryonic stage; incubation day is counted as E0. Development stage estimation was done according to previous studies (Hamburger and Hamilton, 1951; Nagai et al., 2011; Olea and Sandoval, 2012; Murray et al., 2013). Bird sample preparation was performed as previously described (Friocourt et al., 2017). Brains were dissected for samples mentioned in Table S1.

All tissue was fixed in 4% PFA at 4°C overnight, and stored in 1X PBS at 4°C until use.

Human tissue collection and processing.

Human fetuses were obtained with the parent's written informed consent (Gynaecology Hospital Jeanne de Flandres, Lille, France) with approval of the local human ethics committee (protocol N°PFS16-002). Tissues were made available in accordance with French bylaw (Good practice concerning the conservation, transformation and transportation of human tissue to be used therapeutically, published on December 29, 1998). Permission to utilize human tissues was obtained from the French agency for biomedical research (Agence de la Biomédecine, Saint-Denis La Plaine, France). Fetuses were fixed by immersion in 4% PFA at 4°C for 1 to 5 days depending on size, dissected after fixation and post-fixed in 4% PFA at 4°C overnight.

***In situ* hybridization.**

Antisense riboprobes were labeled with digoxigenin-11-D-UTP (Roche) by *in vitro* transcription of mouse Robo3 exon 12-14 cDNA (Renier et al., 2010). *In situ* hybridization was performed on cryostat sections of mouse embryonic tissue or dissected nervous system as previously described (Marillat et al., 2002). Control sense probe yielded no signal.

Immunostaining.

In toto immunostaining of amniote embryos were performed as described previously (Belle et al., 2017). Briefly, all embryos (except mouse embryos younger than E13 and bird embryos younger than E4/HH25) were dehydrated in methanol, treated overnight at 4°C with a 5% hydrogen peroxide solution in 100% methanol, and rehydrate in methanol to suppress blood autofluorescence and hematomas. Tissues

were conditioned and blocked for 24 h in PBS containing 0.2% gelatin (BDH Prolabo), and 0.5% Triton X-100 (Sigma-Aldrich) (PBSGT) under agitation at room temperature. They were then transferred in PBSGT solution containing 0.1% saponin (10 mg/mL) and primary antibodies, and incubated at 37°C with rotation at 70 rpm, for 7 to 14 days depending on tissue size. Primary antibodies used are Goat anti-human Robo3 (RRID: AB_2181865), Rabbit anti-Foxp2 (RRID: AB_2107107), Gaot anti-Foxp2 (RRID: AB_2107124), Rabbit anti-Barhl1 (RRID: AB_1078266), Rabbit anti-Pax6 (RRID: AB_2315065), Rabbit anti-Islet-1 (RRID: AB_881306), Mouse anti-Neuronal Class III beta-Tubulin (RRID: AB_2313773), Rabbit anti-beta-Tubulin III (RRID: AB_262133). Details and working dilution used in this study are listed in **Table 1**. Samples were washed over one day at room temperature with agitation in PBSGT. Then, tissues were incubated in PBSGT solution containing 0.1% saponin and secondary antibodies, and incubated at 37°C with rotation at 70 rpm overnight. Secondary antibodies used are AffiniPure Bovine anti-goat IgG (H+L) Cy3 (RRID: AB_2340880), Donkey anti-goat IgG (H+L) Alexa Fluor 647 (RRID: AB_2340885), AffiniPure Donkey anti-rabbit IgG (H+L) Cy3 (RRID: AB_2307443), AffiniPure Donkey anti-rabbit IgG (H+L) Alexa Fluor 647 (RRID: AB_2492288), details and working dilution are listed in **Table 2**. Samples were finally washed for two days at room temperature with agitation with multiple PBSGT baths. Samples were then cleared using protocol detailed bellow. Small samples were embedded in agarose prior to clearing as previously described (Belle et al., 2014). Sections immunostaining was performed as previously described (Marillat et al., 2002), using same primary and secondary antibodies used for *in toto* immunostaining, plus Mouse anti-Nestin antibody (Alexa Fluor 488, RRID: AB_2732861) (**Table 1**), and Hoechst (ThermoFisher scientific Cat# 33342, RRID: AB_2651135).

Tissue Clearing.

All tissue, except from human tissue, was cleared using adapted 3DISCO clearing protocol as previously described (Ertürk et al., 2012; Belle et al., 2014). Human tissue was cleared using a methanol clearing protocol adapted from iDisco+ clearing protocol, as described before (Renier et al., 2016; Belle et al., 2017). Samples were stored in dibenzylether (DBE) in light-protected glass vials at room temperature.

Imaging.

3D imaging was performed with an ultramicroscope I (LaVision BioTec) using ImspectorPro software (LaVision BioTec). The light sheet was generated by a laser (wavelength 488 and 561 nm, Coherent Sapphire Laser and 640 nm, Coherent OBIS 640-100LX laser, LaVision BioTec). A binocular stereomicroscope (MXV10, Olympus) with a 2X objective (MVPLAPO, Olympus) was used at different magnifications (0.8x, 1x, 1.25x, 1.6x, 2x, 2.5x, 3.2x, 4x, 5x and 6.3x). Samples were placed in an imaging reservoir made of 100% quartz (LaVision BioTec) filled with DBE and illuminated from the side by the laser light. Images were acquired with a PCO Edge SCMOS CCD camera (LaVision BioTec). The stepsize between each image was fixed to 1 or 2 µm.

Image processing was performed as previously described (Belle et al., 2017) using Imaris x64 software version 8.0.1, Bitplane (RRID:SCR_007370).

RESULTS

Developmental time-course of Robo3 expression in mouse embryo

We first studied the distribution of the Robo3 receptor in early mouse embryos (E9-10) using whole-mount immunostaining, 3DISCO clearing and 3D light sheet fluorescence microscopy (LSFM) (**Figure 1 and Movie S1**). Robo3 was not detected in E8.5 mouse embryos (data not shown; n = 4). At E9, a few pioneer axonal tracts labeled with the pan-neuronal marker βIII-tubulin (Easter et al., 1993; Mastick and Easter, 1996), have started to grow in the CNS (**Figure 1a**; n = 4). This includes the tract of the mesencephalic nucleus of the trigeminal nerve at the surface of the mesencephalon, and the medial longitudinal fasciculus (Mlf, which originates in the interstitial nucleus of Cajal in the pretectal tegmentum/caudal diencephalon) as previously described (Easter et al., 1993; Mastick and Easter, 1996). At this stage, the first Robo3-immunoreactive (Robo3+) axons extending dorso-ventrally towards the ventral midline, were seen in the rhombencephalon except in rhombomeres 1(r1), r3 and r4 (**Figure 1b-d**; n = 5). However, longitudinal Robo3+ axons, belonging to the Mlf, were also observed extending caudally along the midline from the diencephalon to the rhombencephalon (**Figure 1c**). At E9.5 (n = 6), βIII-Tubulin+ neurons were found at all levels of the CNS but also in the peripheral nervous system such as in the dorsal root ganglia (Drg; **Figure 1e, g**). The number of Robo3+ neurons had significantly increased and they were now present almost all along the rhombencephalon but also in the rostral spinal cord (**Figure 1e-h**). Robo3+ growth cones have reached the floor plate and a few have started to cross the midline, indicating that they are commissural axons (**Figure 1g-h**). Robo3 was also expressed in few axons of the Mlf and could be found in tectobulbar/tectospinal axons in the mesencephalon (and future colliculi), which cross the midline (**Figure 1f**). At E10 (n = 5), the tectobulbar/spinal tracts had expanded and its axons highly expressed Robo3 (**Figure 1i, j**). In the rhombencephalon, Robo3 was found at all

levels except in r0 (isthmus)/r1 and r4 (**Figure 1j, k**). In the spinal cord (**Figure 1i, l**), Robo3 was only found in commissural axons, and extended to more caudal levels, following the known rostro-caudal developmental gradient of neuronal differentiation (Nornes and Das, 1972; Liu et al., 2001). Interestingly, Robo3 was also present in the ventral pallium, at the level of the medial and lateral ganglionic eminences (**Figure 1k**). At E11 (**Figure 1m-n**; n = 5) and E12 (**Figure 1o-p**; n = 3), Robo3 was expressed in commissural axons crossing the midline all along the midbrain, hindbrain and spinal cord (**Figure 1m-q**). As previously shown (Barber et al., 2009), at the level of the forebrain, Robo3 was detected in the ganglionic eminences and in interneurons migrating from it toward the cortex (**Figure 1n, o**). Robo3 was also expressed in olfactory sensory axons forming the olfactory nerve and projecting into the olfactory bulb primordium (**Figure 1o, p**). Robo3 expression in neurons was also detected using *in toto in situ* hybridization on E12 mouse nervous system, showing strong expression of *Robo3* in the rhombic lip in the hindbrain, and weaker expression in Ge, Mes and Sc neurons (**Figure 1q**). Robo3+ axons were found in the fasciculus retroflexus (Fr) which connects medial habenula neurons in the dorsal epithalamus to the interpeduncular nucleus (Ipn) in r1 (Moreno-Bravo et al., 2016). At E14 (n = 4), Robo3 was still expressed in commissural axons in the midbrain, hindbrain and spinal cord but almost absent from the forebrain (**Figure 2a-b**). At this stage, the Fr was the only tract rostral to the midbrain with high levels of Robo3 (**Figure 2a, b**). In the hindbrain, Robo3 was found in axons of deep cerebellar nuclei, which project to the ventral medulla, in the cerebellum ventricular zone (VZ), and more caudally in migrating neurons of the lateral reticular nucleus (LRN; **Figure 2b**). Robo3 was also found in processes extending from the rhombic lip (RL) to the floor plate and belonging to future pontine neurons and neurons of brainstem auditory

nuclei (Di Bonito et al., 2013; Zelina et al., 2014). *Robo3* expression in deep cerebellar neurons cerebellum VZ and migrating LRN neurons was detected at E14 using *in situ* hybridization (**Figure 2c-d**). At E16 (n = 8), Robo3 expression was strongly down-regulated in the spinal cord, hindbrain and cerebellum. The only structures expressing Robo3 at this stage were the Fr and the anterior extramural migratory stream (Aems) containing tangentially migrating pontine neurons (**Figure 2e-f**). By E18, the Aems was reduced to a thin stream of *Robo3*+ cells (**Figure 2g**). At E14, habenula neurons start expressing *Robo3* (**Figure 2h**). From E16 to P0, the size of the Fr labeled with Robo3 increased, and as previously shown (Belle et al., 2014) its axons crossed multiple times the floor plate at the level of their target, the Ipn (**Figure 2i-j**). The Fr was the only axonal tract still immunoreactive for Robo3 at birth (**Figure 2j**). These data show specific and transient expression of Robo3 in different axonal tracts during mouse embryogenesis.

Robo3 expression pattern is highly conserved during vertebrate development

Next, we collected embryos from various amniote species to determine if the distribution of the Robo3 receptor during development was evolutionarily conserved (**Figure 3 and Movie S2**).

Early developmental stages

For birds, we immunostained with anti-Robo3 whole embryos from three species belonging to three different orders, the chicken (a galliforme), the duck (an anseriforme), and the zebra finch (a passeriforme). Robo3+ axons could be detected in chicken as early as HH17 embryos (Hamburger and Hamilton, 1951) (n = 4) (**Figure 3a**). Robo3 was present in commissural neurons in the rhombencephalon

and spinal cord, but also, as in the mouse, in axons of the Mlf extending from the caudal diencephalon (**Figure 3a-c**). At HH25 (about 4.5-5 days; n = 5), Robo3 commissural axons spanned the caudal diencephalon, the whole mesencephalon, rhombencephalon, and spinal cord but were absent from the forebrain (**Figure 3d**). Rhombencephalon Robo3 expression dynamics was similar to previous observations in mouse: first at HH17, Robo3 was expressed in rostral and caudal rhombomeres but absent from r3/4 (as identified by cranial nerves position), then Robo3 expression is extended to all rhombencephalon by HH25 (**Figure 3b, d**). This is in agreement with previous studies which showed that the time course of neurogenesis differs between rhombomeres (Keynes and Lumsden, 1990). Robo3 expression pattern was conserved in E4-E6 duck embryos (**Figure 3e, f**; n = 2 and 3, respectively) and E4 and E6 zebra finch embryos (**Figure 3g, h**; n = 4 for each).

For reptiles, we studied embryos from African house snake at 8 days post oviposition (8 dpo, n = 2). Embryos were double stained for βIII-tubulin to visualize all axons and Robo3 (**Figure 3i, j**). As in mouse and birds, Robo3 was seen in commissural axons, from the mesencephalon to the caudal end of the spinal cord and the Mlf was the only non-commissural tract immunoreactive for Robo3.

Next, we studied Robo3 expression in an Australian marsupial, the fat-tailed dunnart (*Sminthopsis crassicaudata*). In dunnart, birth occurs at 13 days of gestation, after which newborns crawl into the mother's pouch and remain attached to the teat until about P40-60 (Dunlop et al., 1997; Suárez et al., 2017). At P2 (n = 2) the youngest stage analyzed, the pattern of Robo3+ axons in the dunnart was highly similar to that of an E13 mouse embryo (**Figure 3k-l**). Robo3 was present in commissural axons from the midbrain to the spinal cord and in the fasciculus retroflexus.

These results show that overall, the neuronal distribution of Robo3 in amniotes, is conserved both in time and space at early developmental stages. To strengthen this conclusion, we next focused on several developing systems.

Robo3 expression in the developing spinal cord

In situ hybridization with a *Robo3*-specific riboprobe and Robo3 immunostaining on cryosections, showed that in the E9.5 mouse spinal cord, Robo3+ commissural neurons appear in the marginal zone, close to the surface of the dorsal spinal cord (**Figure 4a, e**). At this stage, only a few Robo3+ growth cones have reached the floor plate. As previously shown, Robo3 expression is rapidly down-regulated after midline crossing (Marillat et al., 2004; Sabatier et al., 2004) and therefore, at later developmental ages (**Figure 4b-d**), *Robo3* mRNA was only detected in two symmetrical dorso-ventral bands of newly postmitotic neurons adjacent to the ventricular zone and in small ventral domains probably corresponding to V3 interneurons (Alaynick et al., 2011) whereas older more superficial neurons did not express *Robo3* mRNA anymore (**Figure 4b-d**). At E11, Robo3 immunopositive commissural axons extended within the spinal cord, turning towards the floor plate and avoiding differentiating motor neurons (**Figure 4f**). By contrast, at E12.5, Robo3+ axons followed two distinct pathways, a superficial one under the pia or a deeper one along the edge of the ventricular zone (**Figure 4g**). Only a few commissural neurons still express Robo3 at E14, by the time the last spinal cord neurons are generated (**Figure 4h**) (Nornes and Carry, 1978; Holley et al., 1982).

To compare Robo3 expression in spinal cord commissural axons, we also performed 3D LSFM on whole-mount cleared samples. In E11 mouse spinal cord (n = 5), Robo3 was found all along the rostro-caudal axis and immunolabelled axons were well

aligned and interspaced (**Figure 4i, j**). Likewise, Robo3 was also present in commissural axons of the human fetal spinal cord at gestational week 9 (GW9), the earliest age analyzed (**Figure 4l, m**). However, in human, Robo3+ axons formed narrow fascicles before reaching the midline (**Figure 4l**). At GW9 (n = 1) and GW10 (n = 2), optical sections showed that, as in mice, Robo3+ commissural axons also followed either a superficial or a deep pathway to reach the floor plate and that they avoided the motor column (**Figure 4k, n, o**). Faint expression of Robo3 was still detected at GW12 (n = 1) but lost by GW14 (n = 1) (data not shown). This pattern of expression was strikingly similar in dunnarts (**Figure 4p, q**) and snakes (**Figure 4r-t**), although LSFM images showed that as in mice, Robo3+ axons did not form fascicles before crossing the floor plate. Robo3 expression in the dunnart spinal cord was detected until P8 (n = 4), but was absent at P10 (n = 4) (data not shown). In chick embryos, Robo3+ commissural axons formed fascicles at early stages (HH24, n = 4; **Figure 4u, v**), but at older stages (HH28 and HH30; n = 2 and 1) they were highly defasciculated, particularly in the dorsal spinal cord and only met at the floor plate (**Figure 4w,x**). A similar observation was made in sections from E17 ostrich spinal cord (**Figure 4y**; n = 1). Robo3 expression in chicken spinal cord commissural axons was substantially reduced by HH30, and it was undetectable in HH32 embryos (data not shown), consistent with previous observations in other amniote species. These results strongly suggest that the selective transient expression of Robo3 in developing commissural axons of the spinal cord is an ancient feature conserved throughout amniotes.

Robo3, a conserved marker of the developing fasciculus retroflexus

The fasciculus retroflexus (Fr) exists in all vertebrates (Figdor and Stern, 1993; Beretta et al., 2012) and carries axons from the habenula that cross the floor plate at multiple points upon reaching the interpeduncular nucleus in rhombomere 1 (Iwahori et al., 1993; Bianco and Wilson, 2009). In E16 mouse embryos (n = 8), Robo3 was expressed in neurons of the medial habenula and axons of the Fr (**Figure 5a-c, Figure S1a-b, and Movie S3**), as previously shown (Belle et al., 2014). The pattern of Robo3 immunostaining in the habenula was similar in the dunnart (**Figure 5d-f, and Figure S1c-d**), with Robo3+ axons forming a compact tract on each side of the brain extending toward the Ipn. However, at the midline, the crossing pattern was different from the mouse with a noticeable defasciculation, and massive branching of the Fr at the level of the Ipn, followed by a caudal spreading of Robo3+ axons along the midline (**Figure 5f**). In GW8.5-GW11 human fetal brains, both the habenula and Fr axons strongly expressed Robo3 (**Figure 5g-i, and Figure S1e-g**). At GW8.5, the Fr was still thin and just reached the floor plate (**Figure S1e**) but its size increased significantly between GW9-GW11. Interestingly, from GW10, a small Robo3+ commissure was observed crossing the dorsal midline and likely connecting the two human habenular nuclei, which was not present in any of the other species examined (**Figure 5h, i**). At the level of the Ipn, Fr axons defasciculated and crossed the floor plate in a pattern similar to dunnarts. In the snake, the Fr was also Robo3+ at 6 dpo and 10 dpo (**Figure 5j, k**) but unlike in mammals, Fr axons did not form a highly fasciculated tract until they reached the Ipn. Interestingly, multiple arrays of Robo3 fascicles connecting the habenula to the Ipn were also observed in all bird species examined, including chicken (**Figure 5l, m and Figure S1h-i**) and pigeon (**Figure 5n, o**) embryos. At the level of the Ipn, crossing of the midline was also extensive (**Figure 5m, o, q**), but axons did not appear to zig-zag as in mice.

Robo3 expression in the mammalian forebrain and diencephalic tegmentum

Robo3 is not only expressed by commissural axons throughout the hindbrain and spinal cord and in the habenula, but was also found in a few neuronal systems at more rostral levels within the forebrain. In E11 and E12 mouse embryo, Robo3 was present in olfactory sensory axons as they enter the olfactory bulb primordium (**Figure 6a-d**). It was also highly expressed in neurons lining the medial and lateral ganglionic eminence of the telencephalon (**Figure 6f, g**). The presence of Robo3 at this level and in the cortical plate was confirmed using *in situ* hybridization for Robo3 (**Figure 6e**) in agreement with previous reports (e.g.(Barber et al., 2009)). We were also able to extend these observations to the human fetus and the dunnart. At GW9 and GW10 Robo3 presence at the level of the ganglionic eminences was clearly visible in human (**Figure 6h-i**). In the dunnart, cryosection immunostaining shows expression of Robo3 in olfactory nerve axons of P2 dunnart, (**Figure 6j**), which was absent by P4. Interestingly, however, Robo3 expression was not detected in olfactory sensory axons or embryonic forerunners of striatum and pallidum from bird embryos (data not shown).

More caudally, a small Robo3+ ventral axonal tract extending longitudinally between the diencephalic to the mesencephalic tegmentum was also observed in E11 mouse embryo (n = 3), P8 and P10 dunnart (n = 3) and HH25 chick embryo (n = 4) (**Figure 6k-m**). As for other axonal tracts, this expression was transient, as it was not observed at later stages: E14 mouse, P12 dunnart and HH30 chicken embryo (data not shown).

Robo3 expression in the cerebellar and precerebellar systems

During vertebrate evolution, the acquisition of increasingly complex motor skills has been accompanied by a dramatic expansion of the cerebellar system (Butts et al., 2011; Barton, 2012), which includes the cerebellum and precerebellar neurons located in the brainstem and spinal cord.

Deep cerebellar nuclei, the main cerebellum outputs, comprise both ipsilaterally and contralaterally projecting neurons (Sotelo, 2004). Commissural cerebellar axons cross the midline either at the level of the isthmic floor plate or in the cerebellum to connect to vestibular neurons on the opposite side (Bourrat and Sotelo, 1986; Fink et al., 2006). In rodents, ventrally crossing deep nuclei axons express Robo3 (**Figure 7a-c**) and they fail to cross in *Robo3* knockout mice (Tamada et al., 2008). To investigate whether these mechanisms are shared between amniotes, we next studied Robo3 expression in the embryonic cerebellum of various species.

We found that Robo3 was strongly expressed in the human fetal cerebellum at GW10 in deep cerebellar nuclei axons projecting to the ventral isthmic midline (**Figure 7d**). Similar projections were also found in P8 and P10 dunnart (**Figure 7e, f**) and HH29 chick embryo (**Figure 7g**). Interestingly, in all these species, axons that project dorsally across the cerebellum midline also expressed Robo3. Moreover, in dunnart, mouse and chicken, Robo3 was also detected in Foxp2 immunoreactive neurons (**Figure 7c, f**), a Purkinje cell marker in rodents and birds (Teramitsu, 2004; Campbell et al., 2009; Fujita and Sugihara, 2012), suggesting that it might also be expressed by this population of non-commissural neurons.

In the brainstem, Robo3 expression pattern was also largely conserved in all amniotes examined (**Figure 7h-o**). Robo3 was present dorsally in a narrow band of neurons adjacent to the ventricular zone lining the fourth ventricle (**Figure 7h-o**), which projected axons ventrally towards the floor plate, suggesting their commissural

identity. Interestingly, many Robo3+ commissural axons followed a circumferential path but the others projected ventrally, parallel to the floor plate and only turned towards it upon reaching the base of the brainstem without fasciculating. Superficially growing Robo3+ axons probably belong to precerebellar neurons. We have previously shown that in the mouse embryo, Robo3 is expressed by all precerebellar neurons, which comprise mossy fiber projection neurons, such as the lateral reticular nucleus (LRN), external cuneatus nucleus (ECN), pontine nucleus (Pn), and climbing fiber projection neurons of the inferior olivary nucleus (ION) (Marillat et al., 2004; Stanco and Anton, 2013; Zelina et al., 2014). All these neurons are generated in the rhombic lip, a germinative neuroepithelium lining the edges of the fourth ventricle, first described in human embryos (His, 1891; Ray and Dymecki, 2009) They migrate tangentially and superficially towards the floor plate. ION and Pn cells stop at the midline whereas LRN and ECN neurons cross it to settle dorsally on the contralateral side (Stanco and Anton, 2013).

In E13.5-E15 mouse embryos (n = 2 and n = 6) Robo3 was detected caudally and rostrally in two superficial migratory streams corresponding respectively to the LRN/ECN nuclei and Pn neurons (**Figure 8a-c**). The identification of the LRN/ECN stream was confirmed using double labeling for Foxp2, a marker of mouse ION neurons (Belle et al., 2014). LRN/ECN are known to migrate across the floor plate between the ION and the pial surface (**Figure 8b**). At E16, the Foxp2+ ION was still visible but Robo3 was absent from post-migratory ECN/LRN neurons (**Figure 8d**). It was still highly expressed rostrally in the anterior extramural stream (Aems; (Altman and Bayer, 1987)) which contains migrating Pn neurons (**Figure 8d**, see below).

A similar pattern of expression was seen in the hindbrain of human fetuses (n = 3). Robo3 was present in both the caudal and rostral streams at GW9 and GW10

(**Figure 8e, g**). The migrating ION could also be visualized using Foxp2 immunostaining (**Figure 8f**) and underwent a rapid medial aggregation between GW9 and GW10 (**Figure 8h**). They did not express Robo3 at these stages.

In dunnarts, the final phase of ION migration could also be captured using Foxp2 immunostaining between P4-P10 (**Figure 8i-l**), but during this phase the ION did not express Robo3 anymore. By contrast, it was strongly expressed in migrating LRN/ECN neurons, which occupied the same position as in mouse and human embryos. In HH28 chick embryo (**Figure 8m-n**), migrating ION neurons had not yet reached the floor plate and they were intermingled with Robo3+ commissural processes suggesting that some corresponded to the leading processes of ION neurons. At this stage, some Foxp2+ cells were still present in the rhombic lip, and colocalized with Robo3 expression, demonstrating early expression of Robo3 in ION neurons, before they started migrating ventrally (**Figure 8n**).

We were able to study this process in bird species with a wide phylogenetic range, including palaeognathae, galloanserae and neoaves. In E8 duck embryos (n = 2), Robo3+ processes span the entire length of the Foxp2+ ION (**Figure 8o**). By E10, Robo3 staining was only overlapping with the caudal part of the ION and cross sections confirmed that at this stage only a migratory stream of neurons probably corresponding to the equivalent of LRN/ECN still expressed Robo3 (**Figure 8p, q**). In E13-E16 emu embryos, the ION and ECN were also visible using whole-mount staining for Robo3 and Foxp2, but only the latter expressed Robo3 (**Figure 8r-t**). A comparable distribution of both proteins was seen in E7 embryos from pigeon and zebra finch (**Figure 8u, v**). Together, these data suggest that Robo3 is transiently expressed in ION and ECN neurons in all amniotes and both that their migratory pathways and mode of migration are evolutionarily conserved.

As mentioned before, in mouse embryos, the Aems is the last neuronal population to express Robo3 in the brainstem. Accordingly, at E16 only the Aems and Fr were still Robo3 immunoreactive (**Figure 9a, b and Movie S4**) whereas at E15, the migrating LRN was still visible. In E15-E16 mouse, the LRN/ECN and Pn express the transcription factors Barhl1 and Pax6 whereas the ION express FoxP2 (**Figure 9a-c**). In GW10 human fetus, the Aems strongly expressed Robo3, and it formed a continuum between the caudal rhombic lip and the rostral floor plate (**Figure 9d, e and Figure S2a, b**). Rostral migration of Pn neurons expressing Robo3 was still visible at GW11 (**Figure 9f**). This rostral migratory stream was also observed in P10-P15 dunnart (**Figure 9g-k and Figure S2c-e and Movie S4**). First, Barhl1+/Pax6+/Robo3+ Pn neurons migrated ventrally along the rostro-caudal axis of the rhombic lip around the roots of the vestibular and trigeminal nerves. Next, Pn neurons joined to constitute a single stream as they made their final ventral turn towards midline as occurs in mouse embryos (**Figure 9h-k**). Barhl1+ neurons reached the floor plate and aggregated next to it, however these neurons do not express Robo3 any longer when they aggregate as previously described in mouse embryo (Marillat et al., 2004) (**Figure S3a-f**). These results show that the migration pathway of Pn neurons is conserved between eutherian mammals and marsupials.

In vertebrates, pontine neurons are thought to only exist in mammals and some bird species (Puelles et al., 2007; Ray and Dymecki, 2009; Butts et al., 2011; Wullimann, 2011). Therefore, we finally tried to visualize the Aems in bird embryos using Robo3, Barhl1 and Pax6, all of which are markers expressed in the mammalian Aems. In chick embryos, surprisingly, Robo3+ commissural neurons of the caudal hindbrain (in the ION region) were not Pax6+ (**Figure 10a-g**). However, Robo3 was seen in neurons of the intermediate hindbrain, migrating tangentially and crossing ventral

midline, reminiscent of LRN neurons in mammals (**Figure 10f, g**). Although Pax6+ and Barhl+ neurons were also present in the hindbrain (rhombomeres 5/6), they never formed, at any developmental stage, a rostrally migrating Aems and compact pontine nucleus similar to mammals. Accordingly, Robo3+ potential pontine processes and axons directly projected ventrally through the rhombomeres where they originate without following an initial anterior path across several rhombomeres upon leaving the rhombic lip as they do in mice (**Figure 10c**). The same observations were made in 9 day-old pigeon embryos (n = 3). Pax6+/Robo3+ cells were observed in a large medial domain of the ventral hindbrain (in addition to granule cells in the cerebellum) forming narrow and superficial migratory chains, but not an Aems (**Figure 10h-k and Figure S2f, g and Movie S4**). The absence of a typical Aems was confirmed in four other bird embryos, the duck (**Figure 10 l, m**), the ostrich (**Figure 10n, o**), the emu (data not shown) and the zebra finch (**Figure S2h, i**). Of note, in all bird embryos examined, except the ostrich, the Pax6+ cells always settled in the hindbrain at a large distance from the Ipn (visualized using Robo3 as a marker of Fr terminals in the Ipn), whereas in mammals the Pax6+ neurons finish their migration just behind the Ipn (**Figure 10c, k, m, o**). These data suggest that in birds, pontine neurons migrate similarly to LRN/ECN neurons without forming a compact Aems. In support of this conclusion, the observation of Robo3/Pax6 labeling in late pigeon and chick embryos, showed that most Pax6+ cells aggregated in diffuse nuclei most often at a distance from the midline (**Figure 10p-t and Figure S3g-l**). The shape and position of these nuclei matches previous descriptions of the medial and lateral pontine nucleus, and raphe nucleus (Harkmark, 1954; Clarke, 1977).

DISCUSSION

Since its discovery in 2004 (Jen et al., 2004; Sabatier et al., 2004), the Robo3 receptor has emerged as a pivotal regulator of the development of mammalian commissural projections. A *Robo3* gene exists in all vertebrates but whether it plays a similar function in mammals and non-mammalian species is unclear (Friocourt and Chédotal, 2017). In zebrafish, several isoforms of Robo3 have been described and *Robo3* mutant fish exhibit mild commissural axon midline crossing defects (Burgess et al., 2009). Some longitudinally projecting axons are also affected in Robo3 mutant fish, and *Robo3* mRNA is present in non-commissural neurons in the zebrafish CNS (Lee et al., 2001; Challa et al., 2005; Kastenhuber et al., 2009; Zelina et al., 2014) suggesting that Robo3 expression pattern might differ between mammals and other vertebrates. However, preliminary studies in birds showed that Robo3 was present in at least some commissural neurons (Philipp et al., 2012; Friocourt et al., 2017). Here, we have combined whole-mount immunostaining and 3D imaging to study the spatiotemporal expression pattern of the Robo3 receptor in developing amniotes. Our results show that in birds, reptiles, eutherians and marsupials, Robo3 receptor distribution in the developing CNS is highly conserved. First, Robo3 is expressed by most if not all commissural axons in the mesencephalon, rhombencephalon and spinal cord and, to the noticeable exceptions of the fasciculus retroflexus and the human habenular commissure, it is absent from diencephalic and telencephalic commissural tracts. This indicates that Robo3 expression in commissural axons is restricted to those crossing the midline at the level of the floor plate. One exception was found in the cerebellum, where some Robo3-immunoreactive deep nuclei axons cross the roof plate dorsally, within the cerebellum. This suggests that Robo3 regulates midline crossing both at the floor plate and roof plate level, in contrast with

previous data which failed to detect Robo3 in a small population of mouse spinal cord axons crossing the midline dorsally (Comer et al., 2015). The sequence and pattern of Robo3 expression in most commissures appears similar between amniotes. A second feature conserved in amniotes is that Robo3 expression in commissural axons is transient and rapidly down-regulated after axons have crossed the floor plate, except in the fasciculus retroflexus. The molecular mechanisms behind the down-regulation of Robo3 are completely unknown but our data suggest that they could be similar in all amniotes. A third characteristic of Robo3 expression, at least in mammals and birds is its presence on a few non-commissural early axonal tracts, such as the medial longitudinal fasciculus and the olfactory nerve. Together, these results show that Robo3 expression in the amniote CNS is tightly regulated, both spatially and temporally, supporting the existence of a specific and conserved genetic program. However, not much is known about the transcriptional regulation of Robo3 expression, and no transcription factors are shared by all Robo3 expressing neurons (Friocourt and Chédotal, 2017).

Importantly, we also provide evidence for at least one mammalian-specific feature of Robo3, related to its transient expression at the level of the ganglionic eminences. A previous study had shown that Robo3 is expressed in the ganglionic eminences of mouse embryos and that it controls the migration of cortical interneurons (Barber et al., 2009). Our results extend this observation to human fetuses and early postnatal marsupials and it would be interesting to determine if horizontal gaze with progressive scoliosis patients, who carry mutations in Robo3, have neurological symptoms, such as epilepsy, previously linked to abnormal cortical interneuron development.

A better understanding of the possible role played by Robo3 in the evolution of commissural systems in all amniotes will require an extended analysis to other tetrapods such as turtles (testudines) and crocodilians. It will also be important to visualize Robo3-expressing axons in anamniote vertebrates such as amphibians and fish, but this will require the development of specific antibodies as the commercially available ones do not seem to work in these species (data not shown). We previously showed that Robo3 has been positively selected in mammals and that mutations targeting its extracellular domain have abolished the ability of mammalian Robo3 to bind Slit ligands (Zelina et al., 2014). In addition, unlike Robo3 receptor in other vertebrates, mammalian Robo3 can be activated by Netrin-1. Surprisingly, despite this major functional switch, the same neuronal populations express Robo3 in all amniote embryos tested and Robo3 expression is downregulated. This suggests that other molecular pathways might have co-evolved in commissural neurons to cope with these changes, and that Robo3 is essential for commissural axons development. It will be essential to perform loss-of-function mutations of Robo3 receptors in various vertebrate species to assess its role in the development and evolution of commissures.

Importantly, our comparative study also provides new information about the evolution of additional commissural circuits, such as the exclusive expression of Robo3 in the habenular commissure of human fetuses. Additional findings on hindbrain precerebellar nuclei are also particularly unexpected. We could confirm that an inferior olivary nucleus (which always expressed FoxP2) is found in all amniotes and that olivary neurons migrate ventrally from the rhombic lip (Kooy, 1917; Harkmark, 1954; Bangma and Donkelaar, 1982; Gonzalez et al., 1984; Azizi and Woodward, 1987). However, our results suggest that the migration of the neurons of the pontine

nuclei significantly differs between mammals and birds. In mammals, the mature pons is localized close to the floor plate, at the pontine flexure, close to the midbrain-hindbrain boundary. Pontine neurons project mossy fiber axons to cerebellar granule cells. Previous anatomical studies suggested that the pons is absent from all anamniotes but exist in birds (Clarke, 1977; Puelles et al., 2007; Wullimann, 2011). This conclusion is primarily based on axonal tracing and axonal degeneration studies which identified several groups of cells (medial and lateral) in a ventral hindbrain domain more or less corresponding to the expected position of the pons (Brodal et al., 1928; Craigie, 1930; Clarke, 1977; Armstrong and Clarke, 1979). In addition, anatomical, ablation and transplantation studies in chick embryos have shown that these precerebellar neurons are generated in the dorsal hindbrain (His, 1891; Essick, 1912; Harkmark, 1954; Tan and Le Douarin, 1991). Mammalian pontine neurons are generated at more caudal levels than their final position and migrate anteriorly in a compact stream (the anterior extramural migratory stream or Aems) across several rhombomeres (Altman and Bayer, 1987; Geisen et al., 2008; Ray and Dymecki, 2009). We observed this stream in mice, humans and fat-tail dunnarts using immunostaining for Robo3, Pax6 and Barhl1 (Landsberg et al., 2005; Zelina et al., 2014). This was not the case in any of the bird species studied, in which only small chains of Pax6/Barhl1/Robo3 neurons were seen, migrating ventrally in a rather straight direction without apparent crossing of rhombomere boundaries, and not approaching the interpeduncular nucleus as in mammals. This is consistent with embryological data that also failed to provide evidence for trans-rhombomeric migration of putative pontine neurons in chick embryos (Cambronero and Puelles, 2000). Moreover, Pax6+ neurons did not aggregate in a compact nucleus in birds and did not express Robo3 much later than other hindbrain neurons in contrast with

mammals. In conclusion, our data suggest that the Aems has no clear homologue in birds. This also confirms that Robo3 expression is a valuable tool to study the evolution of commissural projections in vertebrates.

CONFLICT OF INTEREST

The authors declare no conflict of interest.

REFERENCES

Aboitiz F, Montiel J. 2003. One hundred million years of interhemispheric communication: the history of the corpus callosum. Braz J Med Biol Res 36:409–420.

Alaynick WA, Jessell TM, Pfaff SL. 2011. SnapShot: Spinal Cord Development. Cell 146:178–178.e1.

Altman J, Bayer S a. 1987. Development of the precerebellar nuclei in the rat: IV. The anterior precerebellar extramural migratory stream and the nucleus reticularis tegmenti pontis and the basal pontine gray. J Comp Neurol 257:529–52.

Armstrong RC, Clarke PG. 1979. Neuronal death and the development of the pontine nuclei and inferior olive in the chick. Neuroscience 4:1635–47.

Azizi S a, Woodward DJ. 1987. Inferior olivary nuclear complex of the rat: morphology and comments on the principles of organization within the olivocerebellar system. J Comp Neurol 263:467–484.

Bangma GC, Donkelaar HJ Ten. 1982. Afferent connections of the cerebellum in various types of reptiles. J Comp Neurol 207:255–273.

Barber M, Di Meglio T, Andrews WD, Hernández-Miranda LR, Murakami F, Chédotal A, Parnavelas JG. 2009. The role of Robo3 in the development of cortical interneurons. Cereb cortex 19 Suppl 1:i22-31.

Barton R a. 2012. Embodied cognitive evolution and the cerebellum. Philos Trans R Soc Lond B Biol Sci 367:2097–107.

Belle M, Godefroy D, Couly G, Malone SA, Collier F, Giacobini P, Chédotal A. 2017. Tridimensional Visualization and Analysis of Early Human Development. Cell 169:161–173.e12.

Belle M, Godefroy D, Dominici C, Heitz-Marchaland C, Zelina P, Hellal F, Bradke F, Chédotal A. 2014. A Simple Method for 3D Analysis of Immunolabeled Axonal Tracts in a Transparent Nervous System. Cell Rep 9:1191–1201.

Beretta C a, Dross N, Guiterrez-Triana J a, Ryu S, Carl M. 2012. Habenula circuit development: past, present, and future. Front Neurosci 6:51.

Bianco IH, Wilson SW. 2009. The habenular nuclei: a conserved asymmetric relay station in the vertebrate brain. Philos Trans R Soc B Biol Sci 364:1005–1020.

Boback SM, Dichter EK, Mistry HL. 2012. A developmental staging series for the African house snake, Boaedon (Lamprophis) fuliginosus. Zoology 115:38–46.

Di Bonito M, Narita Y, Avallone B, Sequino L, Mancuso M, Andolfi G, Franzè AM, Puelles L, Rijli FM, Studer M. 2013. Assembly of the auditory circuitry by a hox genetic network in the mouse brainstem. PLoS Genet 9:e1003249.

Bourrat F, Sotelo C. 1986. Neuronal migration and dendritic maturation of the medial cerebellar nucleus in rat embryos: an HRP in vitro study using cerebellar slabs. Brain Res 378:69–85.

Brodal A, Kristiansen K, Jansen J. 1928. experimental demonstration of a pontine homologue in birds. J Comp Neurol 92:23–69.

Brown WS, Jeeves MA, Dietrich R, Burnison DS. 1999. Bilateral field advantage and evoked potential interhemispheric transmission in commissurotomy and callosal agenesis. Neuropsychologia 37:1165–1180.

Burgess HA, Johnson SL, Granato M. 2009. Unidirectional startle responses and disrupted left-right co-ordination of motor behaviors in robo3 mutant zebrafish. Genes, Brain Behav 8:500–511.

Butts T, Chaplin N, Wingate RJT. 2011. Can clues from evolution unlock the molecular development of the cerebellum? Mol Neurobiol 43:67–76.

Cambronero F, Puelles L. 2000. Rostrocaudal nuclear relationships in the avian medulla oblongata: a fate map with quail chick chimeras. J Comp Neurol 427:522–45.

Campbell P, Reep RL, Stoll ML, Ophir AG, Phelps SM. 2009. Conservation and diversity of Foxp2 expression in muroid rodents: functional implications. J Comp Neurol 512:84–100.

Challa AK, Beattie CE, Seeger MA. 2001. Identification and characterization of roundabout orthologs in zebrafish. Mech Dev 101:249–253.

Challa AK, McWhorter ML, Wang C, Seeger M a, Beattie CE. 2005. Robo3 isoforms have distinct roles during zebrafish development. Mech Dev 122:1073–86.

Chédotal A. 2011. Further tales of the midline. Curr Opin Neurobiol 21:68–75.

Clarke PG. 1977. Some visual and other connections to the cerebellum of the pigeon. J Comp Neurol 174:535–52.

Comer JD, Pan FC, Willet SG, Haldipur P, Millen KJ, Wright CVE, Kaltschmidt J a. 2015. Sensory and spinal inhibitory dorsal midline crossing is independent of Robo3. Front Neural Circuits 9:1–14.

Craigie E. 1930. Studies on the brain of the kiwi (Apteryx australis). J Comp Neurol 49:223–357.

Di-Poï N, Milinkovitch MC. 2016. The anatomical placode in reptile scale morphogenesis indicates shared ancestry among skin appendages in amniotes. Sci Adv 2:e1600708–e1600708.

Dunlop SA, Tee LBG, Lund RD, Beazley LD. 1997. Development of primary visual projections occurs entirely postnatally in the fat-tailed dunnart, a marsupial mouse,Sminthopsis crassicaudata. J Comp Neurol 384:26–40.

Easter SS, Ross LS, Frankfurter A. 1993. Initial tract formation in the mouse brain. J Neurosci 13:285–99.

Ertürk A, Becker K, Jährling N, Mauch CP, Hojer CD, Egen JG, Hellal F, Bradke F, Sheng M, Dodt H-U. 2012. Three-dimensional imaging of solvent-cleared organs using 3DISCO. Nat Protoc 7:1983–1995.

Escalante A, Murillo B, Morenilla-Palao C, Klar A, Herrera E. 2013. Zic2-Dependent Axon Midline Avoidance Controls the Formation of Major Ipsilateral Tracts in the CNS. Neuron 80:1392–1406.

Essick CR. 1912. The development of the nuclei pontis and the nucleus arcuatus in man. Am J Anat 13:25–54.

Figdor MC, Stern CD. 1993. Segmental organization of embryonic diencephalon. Nature 363:630–634.

Fink AJ, Englund C, Daza R a M, Pham D, Lau C, Nivison M, Kowalczyk T, Hevner RF. 2006. Development of the deep cerebellar nuclei: transcription factors and cell migration from the rhombic lip. J Neurosci 26:3066–76.

Friocourt F, Chédotal A. 2017. The Robo3 receptor, a key player in the development, evolution, and function of commissural systems. Dev Neurobiol 77:876–890.

Friocourt F, Lafont A-G, Kress C, Pain B, Manceau M, Dufour S, Chédotal A, Laffont A-G, Kress C, Pain B, Manceau M, Dufour S, Chédotal A. 2017. Recurrent DCC gene losses during bird evolution. Sci Rep 7:37569.

Fujita H, Sugihara I. 2012. FoxP2 expression in the cerebellum and inferior olive: development of the transverse stripe-shaped expression pattern in the mouse cerebellar cortex. J Comp Neurol 520:656–77.

Geisen MJ, Meglio T Di, Pasqualetti M, Ducret S, Brunet J-F, Chedotal A, Rijli FM. 2008. Hox Paralog Group 2 Genes Control the Migration of Mouse Pontine Neurons through Slit-Robo Signaling. PLoS Biol 6:e142.

Gonzalez A, ten Donkelaar HJ, De Boer-van Huizen R. 1984. Cerebellar connections in Xenopus laevis An HRP study. Anat Embryol (Berl) 169:167–176.

Goulding M. 2009. Circuits controlling vertebrate locomotion: moving in a new direction. Nat Rev Neurosci 10:507–18.

Hamburger V, Hamilton HL. 1951. A series of normal stages in the development of the chick embryo. J Morphol 88:49–92.

Harkmark W. 1954. Cell migrations from the rhombic lip to the inferior olive, the nucleus raphe and the pons. A morphological and experimental investigation of the chick embryo. J Comp Neurol 100:115–209.

His W. 1891. Die Entwickelung des menschlichen Rautenhirns vom Ende des ersten bis zum Beginn des dritten Monats. Abhandlungen der königlich sächsischen Gesellschafi der Wissenschaften, Math Klasse 29:1–74.

Hocking JC, Hehr CL, Bertolesi GE, Wu JY, McFarlane S. 2010. Distinct roles for Robo2 in the regulation of axon and dendrite growth by retinal ganglion cells. Mech Dev 127:36–48.

Holley JA, Nornes HO, Morita M. 1982. Guidance of neuritic growth in the transverse plane of embryonic mouse spinal cord. J Comp Neurol 205:360–370.

Iwahori N, Nakamura K, Kameda S, Tahara H. 1993. Terminal patterns of the tegmental afferents in the interpeduncular nucleus : a Golgi study in the mouse. Anat Embryol (Berl) 188:593–599.

Jamuar SS, Schmitz-Abe K, D'Gama AM, Drottar M, Chan W-M, Peeva M, Servattalab S, Lam A-TN, Delgado MR, Clegg NJ, Zayed Z Al, Dogar MA, Alorainy IA, Jamea AA, Abu-Amero K, Griebel M, Ward W, Lein ES, Markianos K, Barkovich AJ, Robson CD, Grant PE, Bosley TM, Engle EC, Walsh CA, Yu TW. 2017. Biallelic mutations in human DCC cause developmental split-brain syndrome. Nat Genet:1–8.

Jen JC, Chan W-MM, Bosley TM, Wan J, Carr JR, Rub U, Shattuck D, Salamon G, Kudo LC, Ou J, Lin DDM, Salih MAM, Kansu T, Al Dhalaan H, Al Zayed Z, MacDonald DB, Stigsby B, Plaitakis A, Dretakis EK, Gottlob I, Pieh C, Traboulsi EI, Wang Q, Wang L, Andrews C, Yamada K, Demer JL, Karim S, Alger JR, Geschwind DH, Deller T, Sicotte NL, Nelson SF, Baloh RW, Engle EC, Rüb U. 2004. Mutations in a human ROBO gene disrupt hindbrain axon pathway crossing and morphogenesis. Science 304:1509–1513.

Kastenhuber E, Kern U, Bonkowsky JL, Chien C-B, Driever W, Schweitzer J. 2009. Netrin-DCC, Robo-Slit, and heparan sulfate proteoglycans coordinate lateral positioning of longitudinal dopaminergic diencephalospinal axons. J Neurosci 29:8914–26.

Keynes R, Lumsden A. 1990. Segmentation and the Origin of Regional Diversity in the Vertebrate Central Nervous System. Neuron 2:1–9.

Kiehn O. 2016. Decoding the organization of spinal circuits that control locomotion. Nat Rev Neurosci 17:224–238.

Kooy FH. 1917. The inferior olive in vertebrates.

Landsberg RL, Awatramani RB, Hunter NL, Farago AF, DiPietrantonio HJ, Rodriguez CI, Dymecki SM. 2005. Hindbrain rhombic lip is comprised of discrete progenitor cell populations allocated by Pax6. Neuron 48:933–47.

Lee JS, Ray R, Chien CB. 2001. Cloning and expression of three zebrafish roundabout homologs suggest roles in axon guidance and cell migration. Dev Dyn 221:216–30.

Letzner S, Simon A, Güntürkün O. 2016. Connectivity and neurochemistry of the commissura anterior of the pigeon (Columba livia). J Comp Neurol 524:343–361.

Liu J-P, Laufer E, Jessell TM. 2001. Assigning the Positional Identity of Spinal Motor Neurons. Neuron 32:997–1012.

Marillat V, Cases O, Nguyenf-Ba-Charvet KT, Tessier-Lavigne M, Sotelo C, Chédotal A. 2002. Spatiotemporal expression patterns of slit and robo genes in the rat brain. J Comp Neurol 442:130–155.

Marillat V, Sabatier C, Failli V, Matsunaga E, Sotelo C, Tessier-Lavigne M, Chédotal

A. 2004. The Slit Receptor Rig-1/Robo3 Controls Midline Crossing by Hindbrain Precerebellar Neurons and Axons. Neuron 43:69–79.

Martin GR. 2009. What is binocular vision for ? A birds ' eye view. J Vis 9:1–19.

Mastick GS, Easter SS. 1996. Initial organization of neurons and tracts in the embryonic mouse fore- and midbrain. Dev Biol 173:79–94.

Moreno-Bravo J a, Martinez-Lopez JE, Madrigal MP, Kim M, Mastick GS, Lopez-Bendito G, Martinez S, Puelles E. 2016. Developmental guidance of the retroflex tract at its bending point involves Robo1-Slit2-mediated floor plate repulsion. Brain Struct Funct 221:665–678.

Murray JR, Varian-Ramos CW, Welch ZS, Saha MS. 2013. Embryological staging of the Zebra Finch, Taeniopygia guttata. J Morphol 274:1090–1110.

Nagai H, Mak SS, Weng W, Nakaya Y, Ladher R, Sheng G. 2011. Embryonic development of the emu, Dromaius novaehollandiae. Dev Dyn 240:162–175.

Nornes HO, Carry M. 1978. Neurogenesis in spinal cord of mouse: an autoradiographic analysis. Brain Res 159:1–16.

Nornes HO, Das GD. 1972. Temporal Pattern of Neurogenesis in Spinal Cord: Cytoarchitecture and Directed Growth of Axons. Proc Natl Acad Sci 69:1962–1966.

Olea GB, Sandoval MT. 2012. Embryonic development of Columba livia (Aves: Columbiformes) from an altricial-precocial perspective. Rev Colomb Ciencias Pecu 25:3–13.

Paolino A, Fenlon LR, Kozulin P, Richards LJ, Suárez R. 2018. Multiple events of gene manipulation via in pouch electroporation in a marsupial model of

mammalian forebrain development. J Neurosci Methods 293:45–52.

Paterson AK, Bottjer SW. 2017. Cortical inter-hemispheric circuits for multimodal vocal learning in songbirds. J Comp Neurol 525:3312–3340.

Paul LK, Brown WS, Adolphs R, Tyszka JM, Richards LJ, Mukherjee P, Sherr EH. 2007. Agenesis of the corpus callosum: genetic, developmental and functional aspects of connectivity. Nat Rev Neurosci 8:287–299.

Petros TJ, Rebsam A, Mason CA. 2008. Retinal axon growth at the optic chiasm: to cross or not to cross. Annu Rev Neurosci 31:295–315.

Philipp M, Niederkofler V, Debrunner M, Alther T, Kunz B, Stoeckli ET. 2012. RabGDI controls axonal midline crossing by regulating Robo1 surface expression. Neural Dev 7:36.

Puelles L, Martinez-de-la-Torre M, Martinez S, Watson C, Paxinos G. 2007. The Chick Brain in Stereotaxic Coordinates. A Photographic Atlas correlating Avian and Mammalian Neuroanatomy. San Diego: Academic Press.

Ray RS, Dymecki SM. 2009. Rautenlippe Redux -- toward a unified view of the precerebellar rhombic lip. Curr Opin Cell Biol 21:741–7.

Renier N, Adams EL, Kirst C, Wu Z, Azevedo R, Kohl J, Autry AE, Kadiri L, Umadevi Venkataraju K, Zhou Y, Wang VX, Tang CY, Olsen O, Dulac C, Osten P, Tessier-Lavigne M. 2016. Mapping of Brain Activity by Automated Volume Analysis of Immediate Early Genes. Cell 165:1789–1802.

Renier N, Schonewille M, Giraudet F, Badura A, Tessier-Lavigne M, Avan P, De Zeeuw CI, Chédotal A. 2010. Genetic Dissection of the Function of Hindbrain Axonal Commissures. PLoS Biol 8:e1000325.

Sabatier C, Plump AS, Le Ma, Brose K, Tamada A, Murakami F, Lee EY-H., Tessier-Lavigne M. 2004. The Divergent Robo Family Protein Rig-1/Robo3 Is a Negative Regulator of Slit Responsiveness Required for Midline Crossing by Commissural Axons. Cell 117:157–169.

Schweitzer J, Lohr H, Bonkowsky JL, Hubscher K, Driever W, Löhr H, Hübscher K. 2013. Sim1a and Arnt2 contribute to hypothalamo-spinal axon guidance by regulating Robo2 activity via a Robo3-dependent mechanism. Development 140:93–106.

Sotelo C. 2004. Cellular and genetic regulation of the development of the cerebellar system. Prog Neurobiol 72:295–339.

Stanco A, Anton ES. 2013. Radial Migration of Neurons in the Cerebral Cortex. In: Rubenstein JLR, Rakic P, editors. Cellular Migration and Formation of Neuronal Connections. Vol. 2. Elsevier. p 317–330.

Suárez R, Gobius I, Richards LJ. 2014. Evolution and development of interhemispheric connections in the vertebrate forebrain. Front Hum Neurosci 8:497.

Suárez R, Paolino A, Fenlon LR, Morcom LR, Kozulin P, Kurniawan ND, Richards LJ. 2018. A pan-mammalian map of interhemispheric brain connections predates the evolution of the corpus callosum. Proc Natl Acad Sci 115:9622–9627.

Suárez R, Paolino A, Kozulin P, Fenlon LR, Morcom LR, Englebright R, O'Hara PJ, Murray PJ, Richards LJ. 2017. Development of body, head and brain features in the Australian fat-tailed dunnart (Sminthopsis crassicaudata; Marsupialia: Dasyuridae); A postnatal model of forebrain formation. PLoS One 12:1–18.

Tamada A, Kumada T, Zhu Y, Matsumoto T, Hatanaka Y, Muguruma K, Chen Z, Tanabe Y, Torigoe M, Yamauchi K, Oyama H, Nishida K, Murakami F. 2008. Crucial roles of Robo proteins in midline crossing of cerebellofugal axons and lack of their up-regulation after midline crossing. Neural Dev 3:29.

Tan K, Le Douarin NM. 1991. Development of the nuclei and cell migration in the medulla oblongata Application of the quail-chick chimera system. Anat Embryol (Berl) 183:321–343.

Teramitsu I. 2004. Parallel FoxP1 and FoxP2 Expression in Songbird and Human Brain Predicts Functional Interaction. J Neurosci 24:3152–3163.

Welniarz Q, Dusart I, Gallea C, Roze E. 2015. One hand clapping: lateralization of motor control. Front Neuroanat 9:75.

Welniarz Q, Dusart I, Roze E. 2017. The corticospinal tract: Evolution, development, and human disorders. Dev Neurobiol 77:810–829.

Wullimann M. 2011. The long adventurous journey of rhombic lip cells in jawed vertebrates: a comparative developmental analysis. Front Neuroanat 5:27.

Zelina P, Blockus H, Zagar Y, Péres A, Friocourt F, Wu Z, Rama N, Fouquet C, Hohenester E, Tessier-Lavigne M, Schweitzer J, Crollius HR, Chédotal A. 2014. Signaling Switch of the Axon Guidance Receptor Robo3 during Vertebrate Evolution. Neuron 84:1–15.

FIGURE LEGENDS

Figure 1: Robo3 expression in early mouse embryos.

3D visualization of Robo3 (white or red) and βIII-Tubulin (green) expression in E9 (**a-d**), E9.5 (**e-h**), E10 (**i-l**), E11 (**m-n**) and E12 (**o-q**) mouse embryos. **a.** Surface shading of E9 mouse embryo (grey) with βIII-Tubulin labeling overlay (green) displaying the general organization of the central nervous system in mouse embryos. Anatomical landmarks indicate the position of the Forebrain (Fb), Midbrain (Mb), Rhombencephalon (Rho), Spinal cord (Sc), Forelimb bud (Flb) and 1st and 2nd branchial arches (1 and 2). Dashed lines mark Mb/Rho and Rho/Sc borders. **b.** Early Robo3 expression at E9 is restricted to the following areas: Rho (except rhombomeres 0/1 (r0/1), r3 and r4), and longitudinal axons extending from diencephalon to Rho (c). **c.** Magnification of Robo3 expression in diencephalon and Mb. Few cells express Robo3 and extend their axons ipsilaterally towards the rostral Rho (arrowhead). **d.** Lateral view of Robo3 expression in caudal Rho. Dorso-ventral orientation is indicated by the double-headed arrow. A few dorsally-located neurons express Robo3 and extend their axons ventrally towards the midline. Robo3 expression is detected in cell bodies, in axons and growth cones. **e.** At E9.5, Robo3 expression extended to the entire Rho (except the medial rhombomeres), and to the rostral Sc. **f.** Dorsal view of Robo3 expression at Isthmus(r0)/rhombomere1(r1) boundary. Ipsilateral axons of the medial longitudinal fascicule (Mlf), projecting from Mb to Rho, express Robo3 and are indicated by the arrowhead. Robo3 is strongly expressed in commissural axons of Mb and Rho. **g.** Dorsal view of the spinal cord labeled with Robo3 (red); antero-posterior orientation is indicated by the double-headed arrow. Robo3 is expressed by many differentiated neurons of the lateral spinal cord and in the growth cones of pioneer commissural axons extending toward the midline. Robo3 expression is absent from the dorsal root ganglia (Drg) and

peripheral nerves. **h.** Sc optical section at E9.5 illustrating Robo3 expression in commissural axons extending toward the ventral midline (arrowhead). **i.** At E10, Robo3 expression increases in the Mb, Hb, and Sc, where it is expressed in a high-rostral to low-caudal gradient. Weak expression of Robo3 is also detected in the Fb. **j-k.** Lateral (**j**) and fronto-lateral (**k**) visualization of Robo3 expression. Commissural Mb and Hb axons strongly express Robo3 and few Mlf axons are labelled with Robo3. Low expression of Robo3 is also detected in the ganglionic eminences (Ge). **l.** Lateral view of the Sc, showing strong Robo3 labelling in commissural axons extending towards the ventral midline. Robo3 is not expressed in the peripheral nervous system, labelled by βIII-Tubulin staining (green). **m.** At E11, Robo3 is strongly expressed in commissures along all Sc, Hb and Mb, and in few regions in the Fb. **n.** Lateral view illustrating Robo3 expression in the telencephalon including the lateral and medial ganglionic eminences (Ge), cortex (Cx) and a few olfactory nerve axons (asterisk). Robo3 is also expressed in the fasciculus retroflexus (Fr) and other ventral tracts of the diencephalon. Dashed line outlines the head. **o.** At E12, Robo3 expression is continuous from Sc to Mb, including the cerebellar plate (Cb). Low Robo3 expression is still present in Ge and Fr. **p.** Robo3 expression is maintained in the ganglionic eminences and a few olfactory nerve axons (On, arrowhead). **q.** *In situ* hybridization of *Robo3* in dissected mouse central nervous system shows high *Robo3* expression in rhombic lip neurons in Hb at E12, as well as moderate expression in Ge, Mes and Sc neurons. Scale bars and their sizes are indicated in µm on each image.

Figure 2: Robo3 expression in late developmental stages of the mouse.

a. 3D visualization of E14 mouse embryo with surface shading (grey) and Robo3 expression (red overlay). At this stage, Robo3 is expressed in medial habenula (Hab), and in commissural axons in the mesencephalon (Mes), hindbrain (Hb), including the cerebellum (Cb), and spinal cord (Sc). **b.** Dorsal view of Robo3 expression in E14 mouse brain, showing expression in the fasciculus retroflexus (Fr), deep cerebellar nuclei axons (arrow) and migrating lateral reticular nuclei neurons (arrowhead). **c-d.** *In situ* hybridization of *Robo3* on coronal section from E14 mouse embryos showing *Robo3* expression in deep cerebellar neurons (arrow in c), cerebellum ventricular zone (VZ) and migrating lateral reticular nuclei neurons (LRN and arrowhead in **d**) **e.** Dorsal view of Robo3 expression in E14 mouse brain, showing expression in the fasciculus retroflexus (Fr) and anterior extramural migratory stream (Aems). **f.g.** *In toto in situ* hybridization of *Robo3* in dissected mouse brains at E16 (**f**) and E18 (**g**). At E16, *Robo3* expression is still visible in migrating pontine neurons in the Aems. Note that pontine neurons stop expressing *Robo3* before reaching ventral midline. At E18, a faint *Robo3* expression was still detectable in migrating pontine neurons. **h.** *In situ* hybridization of *Robo3* on a coronal section from E14 mouse forebrain showing *Robo3* expression in medial habenula neurons (Hab). **i-j.** Dorsal view of Robo3 expression in habenular neurons at E16 (**i**) and P0 (**j**). Robo3 is expressed in cell bodies from the medial habenula (Hab) and their axons forming the Fasciculus retroflexus (Fr). Fr axons zig-zag at the midline at the level of the interpeduncular nucleus (Ipn). Note that Robo3 is absent from the pons at P0. Scale bars and their sizes are indicated in µm on each image.

Figure 3: Overview of Robo3 expression pattern in various amniotes embryos. **a-d.** 3D visualization of Robo3 expression in HH17 (**a-c**) and HH25 (**d**) chicken

embryos. **a.** Robo3 (red) and βIII-Tubulin (green) expression. At HH17, Robo3 is mainly expressed in commissural axons from rostral spinal cord, hindbrain and midbrain. The frame delineates the area seen at a higher magnification in (**b**). **b.** Robo3 is expressed by a few neurons of the ventral caudal diencephalon (Di), and numerous commissural neurons in the rhombencephalon (Rho). Robo3 is absent from the telencephalon (Tel) and diencephalon (Di). Robo3 expression in the hindbrain differs between rhombomeres. **c.** Dorso-lateral view of medial longitudinal fasciculus axons (Mlf; arrowhead) projecting along the ventral mesencephalon (Me) into the rhombencephalon (Rho). Hindbrain commissural neurons below the Mes/Rho boundary (dash line) strongly express Robo3. **d**. At HH25, Robo3 expression extends to the whole spinal cord (Sc), Hb and Mes, in addition to the cerebellum anlage (Cb). **e-f.** 3D visualization of Robo3 expression in duck embryos at E4 (**e**) and E6 (**f**). As in chicken, Robo3 expression is restricted to commissural tracts in the Mes, Rho and Sc. **g-h.** 3D visualization of Robo3 expression in zebra finch embryos at E4 (**g**) and E6 (**h**). Robo3 is strongly expressed in commissural tracts in the Mes, Rho and Sc. Robo3 expression decreases at later stages, but remains high in the Hb (**h**). **i-j.** 3D visualization of Robo3 expression in 8 dpo snake embryos with surface shading (grey) and βIII-Tub (green) (**i**) or alone (**j**). Robo3 is expressed all along Sc commissural tracts, in Rho and in the fasciculus retroflexus axonal tract from the habenula (Fr). **k-l.** 3D visualization of Robo3 expression in dunnart embryos at P2 with surface shading (grey, **k**) or alone (**l**). Robo3 is strongly expressed by commissural neurons of the Rho and Mes, and weakly expressed in Sc and habenula (Hab). Scale bars and their sizes are indicated in µm on each image.

Figure 4: Spinal cord expression of Robo3 across amniotes.

a-d. *In situ* hybridization for *Robo3* on brachial spinal cord sections from E9.5 (**a**), E11 (**b**), E12.5 (**c**) and E14 (**d**) mouse embryos. *Robo3* is first expressed superficially by a few neurons in the dorsal part of the spinal cord (**a**). At E11 and E12.5, *Robo3* is found dorsally adjacent to the ventricular zone but also ventrally at the level of V3 interneurons (asterisk). At E14, a few *Robo3*+ neurons are observed along the ventricular zone. **e-h.** Robo3 protein distribution (red) in brachial spinal cord sections from E9.5 (**e**), E11 (**f**), E12.5 (**g**) and E14 (**h**) mouse embryos. Robo3 is present in pioneer commissural axons and growth cones. At E9.5 newly born axons grow ventrally at the surface but the most advanced axons start to turn medially and cross the floor plate (arrows, **e**). At E11, Robo3+ axons are fasciculated and pass between the motor column (Mn) and the ventricular zone (Vz) before crossing the midline (**f**). From E12.5 to E14 (**g, h**), commissural axons grow in two distinct pathways (arrows in **g**): a superficial one in the marginal zone or a deep one along the edge of the VZ. **i-j,** LSFM 3D images illustrating Robo3 expression in mouse E11 spinal cord through dorsal (**i**) and lateral (**j**) views. **k.** Robo3 and Isl1 expression in E12.5 spinal cord section. Isl1 specifically label Mn and dorsal root ganglia (Drg). **l-o.** Robo3 expression in human spinal cord visualized by 3D images of dorsal (**l**) and lateral (**m**) views, and optical section at GW9 (**n**). Robo3+ commissural axons form small fascicles before crossing the midline. Optical section at GW9 (**n**) and GW10 (**o**) show Robo3+ axons following either a superficial or a deep pathway, mostly avoiding Mn. **p-q.** 3D lateral visualization (**p**) and optical section (**q**) of Robo3 expression in the dunnart spinal cord at P2. Robo3+ axons follow two distinct ventral pathways, superficial or deep. **r-t.** 3D lateral visualization, from ventral (**r**) and lateral views (**s**), of Robo3 expression in the snake spinal cord at 8dpo, and optical section at 10dpo (**t**). Robo3+ commissural axons do not form fascicles before crossing the midline and

navigate ventrally, in both peripheral and deep pathways. **u-x.** Robo3 expression in chicken spinal cord visualized in 3D at HH24 dorsally (**u**), and in coronal sections at HH24 (**v**), HH28 (**w**) and HH30 (**x**). At HH24, Robo3+ commissural axons form a compact tract. At HH28 and HH30, Robo3+ axons are highly defasciculated in their ventral extension but gather at the midline to form a compact ventral commissure. **y.** Robo3 expression in spinal cord section from E17 ostrich embryo present similar features. Asterisks show Robo3+ neurons in ventral spinal cord sections and optical sections of various species. Scale bars sizes are indicated in µm on each image.

Figure 5: Conserved expression pattern of Robo3 in the habenular system of amniote embryos.

Robo3 immunostaining in the habenular system of mouse (**a-c**), dunnart (**d-f**), human (**g-i**), snake (**j-k**), chicken (**l-m,p-q**) and pigeon (**n-o**) embryos. **a-i.** 3D visualization of mouse (**a**), dunnart (**d**) and human (**g**) brains with surface shading (grey) and Robo3 expression (white) in overlay. In mammals, Robo3 is strongly expressed at late embryonic stages by neurons of the medial habenula (Hab) that project via the *fasciculus retroflexus* (Fr) to the interpeduncular nucleus (Ipn), where they cross the midline. Dorsal Fr views show highly fasciculated axons (**b,e**). Caudal views demonstrate multiple crossing points of habenular axons inside the Ipn (**c,f**), describing a typical figure-eight shape in the mouse. Dorsal (**h**) and lateral (**i**) views of the human habenula at GW10. In human, but not in other vertebrate species, Robo3+ axons connect the right and left medial habenula nuclei (arrowheads). **j-k.** Dorsal (**j**) and lateral (**k**) views of Robo3 expression in habenular neurons in snakes at 6 dpo (**j**) and 10 dpo (**k**). Robo3+ axons leave the habenula in a non-fasciculated manner and gather at the midbrain/hindbrain boundary, where they enter the Ipn. **l-q.**

In chicken (**l-m**) and pigeon (**n-o**), Robo3 is weakly expressed in habenular neurons and their axons are de-fasciculated (**l,n**). Individual axons expressing Robo3 converge in the ventral midbrain (Mb) and enter the Ipn in rhombomere 1 of the hindbrain (Hb) where they cross the midline (**m,o**). At later stages, Robo3 is only detected in medial habenula neurons and their axons projecting to the Ipn (**p-q**). Pn, pontine nucleus. Scale bars and their sizes are indicated in µm on each image.

Figure 6: Robo3 is weakly expressed in different populations of non-commissural neurons in the anterior brain.

a-b. 3D visualization of E11 mouse embryo with surface shading (grey), Robo3 (red) and βIII-Tubulin (green) expression in overlay (**a**) or Robo3 only (**b**) illustrates the position of Robo3 expression in the telencephalon. Robo3 is expressed in the ganglionic eminences (Ge) and olfactory sensory axons in the olfactory nerve (On). **c-d.** Robo3 and βIII-Tubulin expression in the septum (Se) and olfactory sensory axons in coronal sections at E11 (**c**) and E12 (**d**). Oe : Olfactory epithelium. **e.** *In situ* hybridization of *Robo3* on coronal sections of E11 mouse embryo telencephalon. *Robo3* is expressed in the medial (Mge) and lateral (Lge) ganglionic eminences and in some cortical plate (Cp) neurons. Ve: ventricle. **f-g.** Coronal sections showing Robo3 expression in the Mge and Lge in E11 (**f**) and E12 (**g**) mouse embryos. The ventricular zone progenitors are labeled with Nestin (Nes, green). **h-i.** 3D visualization of Robo3 expression in the human ganglionic eminences at GW9 (**h**) and GW10 (**i**) from lateral and ventral views with surface shading (grey) and Robo3 expression (white) in overlay. Robo3 is specifically expressed in Ge at both stages, and in On at GW10 (arrowhead). **j.** Robo3 expression in dunnart. At P2, Robo3 is expressed in olfactory nerve axons (On and arrow) connecting olfactory sensory

neurons in the olfactory epithelium lining the nasal cavity (Nc) to the olfactory bulbs (Ob). **k-m.** Robo3 expression in diencephalic tegmentum (DiTg) tract in mouse (**k**), dunnart (**l**), and chicken (**m**). Scale bars sizes are indicated in µm on each image.

Figure 7: Expression of Robo3 in the cerebellum and hindbrain in amniotes.

a, b. Robo3 (red) and FoxP2 (cyan) expression in mouse brain at E14. **a,** is a lateral view. At this stage, Robo3 is almost absent from the spinal cord (Sc), but remains strong in hindbrain, cerebellum (Cb), and midbrain (Mb). FoxP2 specifically labels Purkinje cells in the Cb and is also expressed by inferior olivary nucleus (ION) in the caudal hindbrain. **b.** Is a dorsal view of the Cerebellum. Deep cerebellar nuclei neurons (Dcn) express Robo3 and project axons (arrowhead) toward the hindbrain ventral midline. Robo3+ axons originating from the medial nucleus also project dorsally and cross the cerebellum midline (arrow). **c.** Robo3 and FoxP2 expression in cerebellar plate at E14 (coronal section). Robo3 is found in Dcn and ventricular zone (Vz) but not in Foxp2+ Purkinje cells (Pc). The arrowhead indicates the axons of the medial Dcn which cross the cerebellum midline and form the hook bundle. **d.** Robo3 expression in human cerebellum at GW10. As in the mouse, Dcn strongly expressed Robo3 and project toward the hindbrain ventral midline (arrowhead). **e-f.** Robo3 expression in dunnart cerebellum at P8 (**e**) and P10 (**f**). Horizontal section of cerebellum at P8 shows Robo3-positive commissural axons going through the anterior peduncle (arrowhead) towards the ventral midline (asterisk). Some Robo3+ axons also cross the dorsal midline and project into the contralateral cerebellum (arrow). At P10, Robo3 expression (red) is high in the Dcn but it is also weakly expressed in Purkinje cells, labeled with FoxP2 (cyan). Robo3+ commissural axons projecting from the cerebellum toward the ventral midline are indicated by an

arrowhead. **g.** Dorsal view of Robo3 expression in chicken cerebellum at HH29. Most Robo3+ axons leave the cerebellar plate to cross the ventral midline in the hindbrain (arrowhead) but a compact Robo3+ axonal bundle also crosses the dorsal midline to connect both cerebellar plates (arrow). **h-o.** Robo3 expression in the ventral hindbrain of human (**h-i**), dunnart (**j-k**), chicken (**l-m**) and pigeon (**n-o**) embryos. Lateral views (**h, j, l, n**) and coronal optic section (**i, k, m, o**) of hindbrains show that Robo3 is expressed all along the antero-posterior axis. Robo3 is present in dorsally located cell bodies and their commissural axons projecting ventrally. Robo3+ commissural axons, grow preferentially at the periphery of the hindbrain, but also in deeper areas. Robo3-expressing axons are not tightly fasciculated in any of these species and form a wide ventral commissure (arrowheads). Scale bars and their sizes are indicated in µm on each image.

Figure 8: Robo3 expression in migrating precerebellar neurons of the inferior olive and lateral reticular nuclei.

a. Ventral view of Robo3 expression pattern in mouse hindbrain at E13.5. Antero-posterior orientation is indicated by the double-headed arrow. **b.** Dorso-caudal view of Robo3 (red) and FoxP2 (cyan) expression in caudal hindbrain at E13.5 as indicated in (**a**). Caudal expression of Robo3 is associated with migrating FoxP2+ neurons of the inferior olivary nucleus (ION). Many Robo3+ axons and neurons belonging to the lateral reticular nucleus (LRN)/external cuneatus nucleus (ECN) migratory stream cross the midline (triangle) between the ION and the pial surface. **c-d.** Ventral view of mouse hindbrain at E15 (**c**) and E16 (**d**). Robo3 expression pattern becomes progressively restricted the Anterior extramural migratory stream (Aems), whereas neurons of the ION are Foxp2+ but do not express Robo3 anymore. **e.**

Ventral view of hindbrain commissural axons in GW9 human fetus labeled for Robo3. **f.** Shows FoxP2+ ION neurons migrating in human caudal hindbrain at GW9 as indicated in (**e**). **g.** Ventral view of a GW11 human fetal hindbrain. Robo3 expression pattern is comparable to an E15 mouse hindbrain. **h.** Ventral view of human ION at GW12, labeled with FoxP2 as indicated in (**g**). **i.** Ventral view of a P4 dunnart hindbrain labeled for Robo3. Robo3 is expressed in commissural neurons of the caudal hindbrain, at the level of ION (labeled with FoxP2). **j-k.** Optical sections of P4 (**j**) and P8 (**k**) dunnart hindbrain as indicated in (**i**). Robo3+ commissural neurons belonging to the LRN/ECN (arrowheads) cross the ventral midline below the FoxP2+ ION. **l.** Ventral view of a P10 dunnart hindbrain illustrating the LRN/ECN migratory stream. **m.** Ventral view of HH28 caudal chicken hindbrain. Robo3 is expressed in migrating FoxP2+ ION neurons. **n.** Robo3 expression in a coronal section of HH28 caudal chicken hindbrain, including migrating ION neurons (arrowhead). Most Robo3-positive axons reach the midline via a peripheral pathway. Fp: Floor plate. **o-q.** Robo3 expression in the caudal hindrain of E8 (**o**) and E10 (**p-q**) duck embryos, E13 (**r**) and E16 (**s-t**) emu embryos and E7 pigeon (**u**) and E7 zebra finch (**v**) embryos. Optical sections at late stages (**q, t**) show Robo3-positive axons/neurons of the LRN/ECN crossing ventral midline between ION and pial surface (arrowheads). Scale bars and their sizes are indicated in µm on each image.

Figure 9: Robo3 is expressed by pontine neurons in the anterior migratory stream in mammals.

a, b. 3D visualization, ventro-lateral view (**a**) and ventral view (**b**), of E16 mouse brains immunostained for Robo3 (red) and Barhl1 (green). Robo3 is strongly expressed, together with Barhl1, in the Anterior extramural migratory stream (Aems),

containing pontine nuclei (Pn) neurons migrating from dorsal Rhombic lip (RL) towards the ventral midline (dashed line). Pn neurons migrate in this stream in two phases (indicated by arrows): first they migrate anteriorly in the dorsal hindbrain until they reach the trigeminal nerve root (asterisk), where (second phase, 2) they turn ventrally to reach ventral midline, just caudal to the interpeduncular nucleus (Ipn). **c.** Pax6 and FoxP2 expression in E16 mouse hindbrain (ventral view). Pax6 is expressed by migrating pontine neurons whereas FoxP2 is expressed in the inferior olivary nucleus (ION). **d.** 3D visualization of Robo3 expression in migrating pontine neurons in GW10 human hindbrain (fronto-lateral view, with shading in grey and Robo3 expression in red overlay). Pn neurons strongly express Robo3 and migrate anteriorly in the Aems. **e.** Dorsal view of Robo3 expression in human hindbrain at GW10. Robo3+ Pn neurons migrate in the Aems in two phases: first anteriorly in a compact stream (1) then ventrally (2) reaching the ventral midline just caudal to the Ipn. **f.** Robo3 expression in GW11 human brain (lateral view). Robo3 specifically label migrating precerebellar neurons in the anterior (Aems) and posterior (Pems) extramural migratory streams. **g.** Robo3 and Barhl1 expression in P12 dunnart hindbrain (Ventral view). Robo3 and Barhl1 are expressed in the Aems and Pems. The two Aems migratory phases are indicated (1 and 2). **h-k.** 3D images (**h**, **i**, lateral views, **j**, **k**, ventral views) of the Aems in P12 (**h**) and P15 (**i**) dunnart. Pontine neurons in the Aems migrate anteriorly around the vestibular nerve root (asterisk), before turning ventrally towards the ventral midline. Pn neurons accumulate along the ventral midline, caudal to the Ipn. Scale bars and their sizes are indicated in µm on each image.

Figure 10: Robo3 expression questions the existence of an anterior extramural migratory stream in birds.

a. Expression of Robo3 and Barhl1 in HH28 chicken hindbrain (Dorsal view). At this stage, Robo3 labels many commissural axons navigating toward midline, especially in the caudal rhombencephalon. Barhl1-positive neurons are present dorsally in the rhombic lip (RL). **b.** Coronal section as indicated in (**a**) shows commissural axons expressing Robo3 and Barhl1-positive neurons in the RL. **c.** 3D visualization (lateral view) of HH31 chicken brain with shading (grey) and with Robo3 (red) and Pax6 (green) labeling in overlay. At this stage, Robo3 is restricted to the fasciculus retroflexus projecting to the interpeduncular nucleus (Ipn) and to a few commissural tracts in the caudal hindbrain. Pax6-positive neurons are spread along the lateral-medial hindbrain, including the cerebellum (Cb) and no Aems is seen. Pax6 is also present in neurons in the mesencephalon (Mes) and telencephalon (Tel). **d-g.** Robo3 expression in HH31 chicken hindbrain, alone (**d,e**) and with Pax6 (**f,g**). Many Pax6-positive neurons migrate ventrally but no compact Aems stream can be seen with either Pax6 or Robo3. By contrast, the posterior extramural migratory stream (Pems) is present caudally. **e,g**, are coronal sections at the level ot the yellow line in **d** and **f**. **h-i.** Robo3, Pax6 and FoxP2 expression in E9 pigeon hindbrain (ventral views). Robo3 is expressed all along the hindbrain, and no well-defined migratory stream is detected. Pax6-positive neurons (green) migrate ventrally and rostral to the inferior olivary nucleus (ION) labeled with FoxP2 (Cyan). Many Pax6-positive neurons cross the ventral midline as observed in chicken (arrowhead) **k.** Lateral view showing the ventral migration of Pax6-positive neurons in multiple chain-like streams (arrow). Robo3 is not strongly expressed in these streams. **l-m.** Ventral and lateral views of Robo3 expression in E10 duck hindbrain. Robo3 is expressed by commissural axons

in the caudal hindbrain. Lateral view (**m**) shows Pax6-positive neurons migrating ventrally without forming any compact stream. Pax6+ cells are also present in the cerebellum (Cb) **n-o.** Ventral and lateral views of Robo3 expression in ostrich hindbrain at E17. Robo3 is expressed broadly in hindbrain commissural axons at this stage. Lateral view (**o**) showing the ventral migration of Pax6-positive neurons, spread along the antero-posterior axis. Rostral migrating Pax6-positive neurons express Robo3 and migrate ventrally caudal to the Ipn. The most caudal Pax6-positive neurons only weakly express Robo3. **p-q.** Robo3 and Pax6 expression in E12 pigeon hindbrain. At this late stage, Robo3 is only detected in habenular axons projecting to the Ipn (**p**). Some chains of Pax6-positive neurons still migrate ventrally (arrow in **q**). **r-t.** Robo3 and Pax6 expression in HH40 chicken hindbrain. **r**, ventral view, **s** and **t** are coronal sections at the level of the yellow lines in **r** . At late stages, Pax6-positive neurons form three main nuclei (1-3) in addition to small neuronal clusters. Scale bars and their sizes are indicated in µm on each image.

Supplementary Figures

Figure S1: Evolution of Robo3 expression in the developing habenula.

a-d. 3D images (lateral views) of E14 and E16 mouse brains (**a, b**) and P10 and P15 dunnart brains (**c, d**) immunostained for Robo3. In both species, Robo3 is expressed in neurons of the medial habenula (Hab) and their axons forming the fasciculus retroflexus (Fr) and projecting to the interpeduncular nucleus (Ipn). Robo3 is also expressed in the Cerebellum (Cb) and migrating pontine neurons (Pn). **e-g.** 3D images (dorsal views) of Robo3 expression in the human habenula at GW8.5 (**e**), GW9 (**f**) and GW11 (**g**). Robo3 is present in the medial habenula (Hab) and fasciculus retroflexus (Fr). **h-i.** 3D images (lateral views) of HH29 (**h**) and HH31 (**i**)

chicken brains stained for Robo3. Robo3 is observed in the medial habenula (Hab) and in the Fr projecting to the Ipn. Fr axons are less fasciculated that in mammals. Scale bars and their sizes are indicated in µm on each image.

Figure S2: Distinct migratory pathways of hindbrain neurons in mammal and bird embryos.

a-b. Robo3 expression in GW10 human fetal hindbrain (ventral views). Robo3 labels lateral reticular nucleus (LRN) neurons migrating along the posterior extramural stream (Pems) in the caudal hindbrain, and pontine nuclei (Pn) neurons migrating along the anterior extramural migratory stream (Aems). Robo3 is also expressed in some ventrally migrating neurons in the rostral hindbrain (arrows in **b**). **c-e.** 3D images (ventral views) of Robo3 expression in P10 (**c**, **d**) and P12 (**d**) dunnart hindbrain. Robo3 is expressed in the Pems, some ventrally migrating neurons at P10 (arrows in **d**), and in the Aems also containing Pax6-positive neurons (frame in **c** showed at a higher magnification in **d**). At P12, Robo3 is still strongly expressed in Aems (**e**) which surrounds the vestibular nerve root (asterisk). **f-g.** In pigeon, Robo3 is expressed at E9 in ventrally migrating neurons and axons all along the antero-posterior axis of the hindbrain (**f**). At E9, Pax6-positive neurons form multiple ventral migratory streams (arrow in **g**). **h-i.** In zebra finch, Robo3 is expressed all along the hindbrain at E8 but at a higher level in the Pems (**h**), when Barhl1-positive neurons migrate ventrally towards the midline. At E10, Robo3 is no longer expressed in the caudal hindbrain and Pax6-positive neurons still migrate towards midline, forming multiple individual chains as in the pigeon (arrows, **i**). Scale bars and their sizes are indicated in µm on each image.

Figure S3: Anatomical comparison of Pax6/Barhl1 hindbrain nuclei between mammals and birds.

a-f. 3D visualization (ventro-lateral view, **a** and **d**) and coronal sections (**b, c** and **e, f**) of E16 mouse brain (**a-c**) and P12 (**e**) and P15 dunnart brains (**d, f**) labeled for Robo3 (red) and Barhl1 (green). In both species Robo3 and Barhl1 are highly expressed in the pontine nucleus (Pn) and anterior extramural migratory stream (Aems). Barhl1 is also expressed in the lateral reticular nucleus (LRN) and cerebellum (Cb). Robo3 is present in the fasciculus retroflexus (Fr). Coronal sections (**b, c, e, f**) show Barhl1+/Robo3+ neurons in the Aems migrating towards the ventral midline (triangle) where they accumulate to form the pontine nuclei (Pn). **g-h.** Ventral views of Pax6 (**g**) and Barhl1 (**h**) expressing nuclei in HH40 chicken brainstem. Three main groups of Pax6+ and Barhl1+ neurons can be identified (1, 2 and 3). Robo3 is only expressed in Fr axons projecting to the Ipn. **i-j.** Hindbrain optical sections, as indicated in (**g,h**) showing the ventral position of Barhl1+/Pax6+ neurons. **k-l.** Ventral views of HH40 chicken (**j**) and E14 pigeon (**k**) hindbrains stained with Foxp2 (cyan) and Barhl1/Pax6. Foxp2 is highly expressed in the inferior olive (ION) whereas Pax6+/Barhl1+ cells are present troughout the brainstem. Scale bars and their sizes are indicated in µm on each image.

Supplementary movies

Movie S1: Robo3 expression during mouse embryonic development. 180° view of Robo3 expression in E9, E9.5, E10, E11, E12, E14 and E16 mouse embryos, using whole-mount immunostaining and 3D light sheet fluorescent microscopy (LSFM). High magnification of Robo3 distribution in several key systems: pre-crossing commissural neurons and axons, and Mlf axons at E9; Ganglionic

eminences and olfactory sensory axons at E12; Cerebellum commissural axons at E14; Medial habenula neurons and axons, and pontine neurons migratory stream at E16. Fr: Fasciculus retroflexus, Hab: Medial habenula, Ipn: interpeduncular nucleus, Mlf : medial longitudinal fasciculus, Pn: pontine nucleus.

Movie S2: Robo3 expression in chicken, snake and dunnart embryos. 360° view of Robo3 expression in chicken, snake and dunnart embryos, using whole-mount immunostaining and 3D light sheet fluorescent microscopy (LSFM). Robo3 (white) and βIII-tubulin (green) expression in HH17 chicken embryo, showing global axonal development at HH17 and Robo3 specific expression in hindbrain commissural axons and Mlf ipsilateral axons. Robo3 general expression in mesencephalon, rhombencephalon and spinal cord commissural axons in HH25 chicken, 8dpo snake and P2 fat-tailled dunnart embryos.

Movie S3: Robo3 expression in mouse, human, dunnart and chicken embryos. 3D visualization of Robo3 expression in mouse, human, dunnart and chicken embryos dissected brains, using whole-mount immunostaining and 3D light sheet fluorescent microscopy (LSFM). High magnification of Robo3 distribution in medial habenula neurons and axons, extending in the fasciculus retroflexus (Fr) and crossing the ventral midline at the level of the interpeduncular nucleus (Ipn). In human, a dorsal commissure bridging medial habenula nuclei is observed.

Movie S4: Robo3 expression in late migrating hindbrain commissural neurons in various amniotes. 3D visualization of Robo3 (red) and Barhl1 or Pax6 (green) expression in dissected brains from mouse, dunnart, and pigeon embryos, using

whole-mount immunostaining and 3D light sheet fluorescent microscopy (LSFM). Neuronal migratory streams are indicated by arrows.

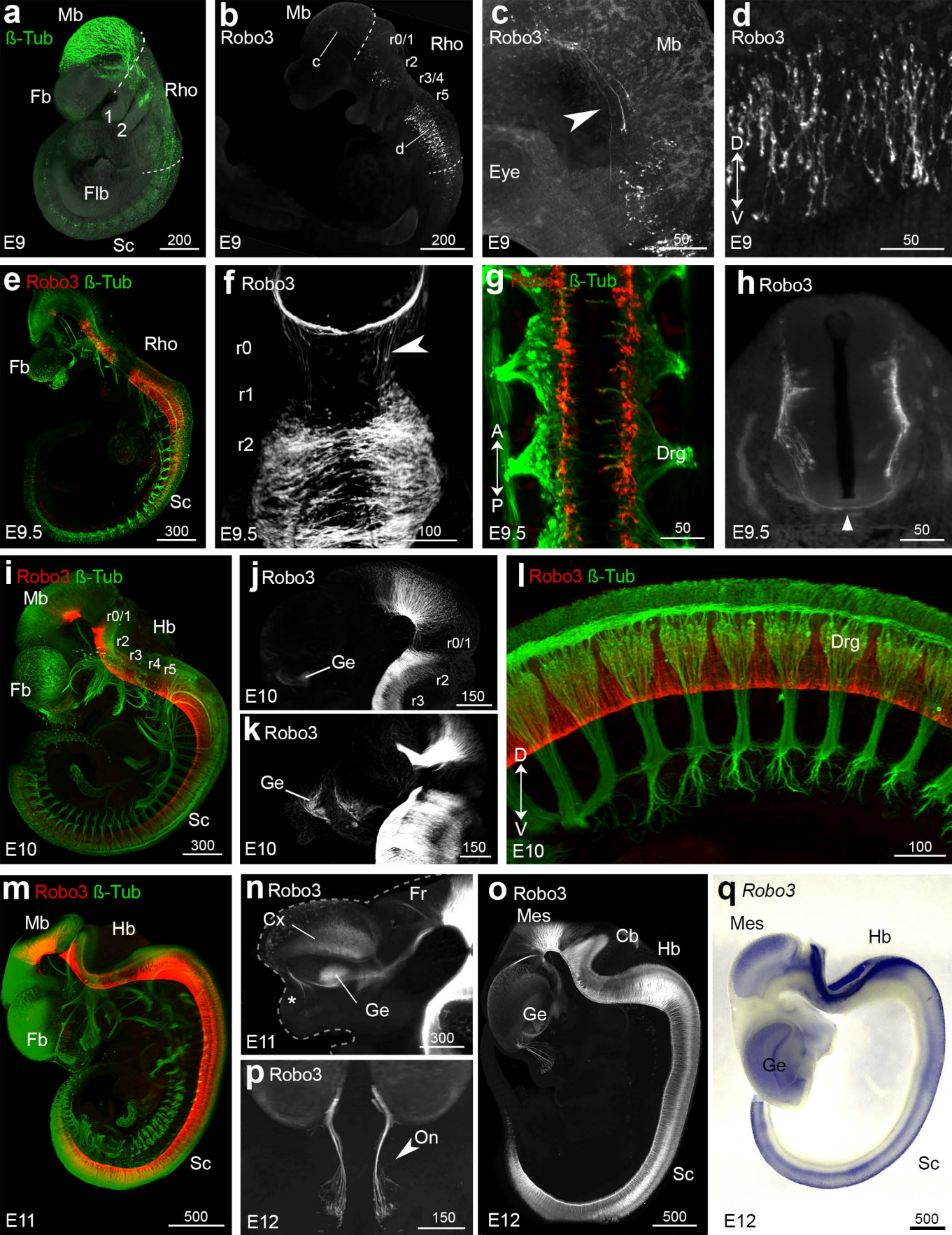
a
Mb
ß-Tub
Fb
Rho
1
2
Flb
E9
Sc
200
b
Mb
Robo3
c
r0/1
Rho
r2
r3/4
r5
d
E9
200
c
Robo3
Mb
Eye
E9
50
d
Robo3
D
V
E9
50
e
Robo3 ß-Tub
Rho
Fb
Sc
E9.5
300
f
Robo3
r0
r1
r2
E9.5
100
g
Robo3 ß-Tub
A
P
Drg
E9.5
50
h
Robo3
E9.5
50
i
Robo3 ß-Tub
Mb
r0/1
Hb
r2
r3
r4
r5
Fb
Sc
E10
300
j
Robo3
r0/1
Ge
r2
r3
E10
150
k
Robo3
Ge
E10
150
l
Robo3 ß-Tub
Drg
D
V
E10
100
m
Robo3 ß-Tub
Mb
Hb
Fb
Sc
E11
500
n
Robo3
Fr
Cx
*
Ge
E11
300
o
Robo3
Mes
Cb
Hb
Ge
Sc
E12
500
p
Robo3
On
E12
150
q
Robo3
Mes
Hb
Ge
Sc
E12
500

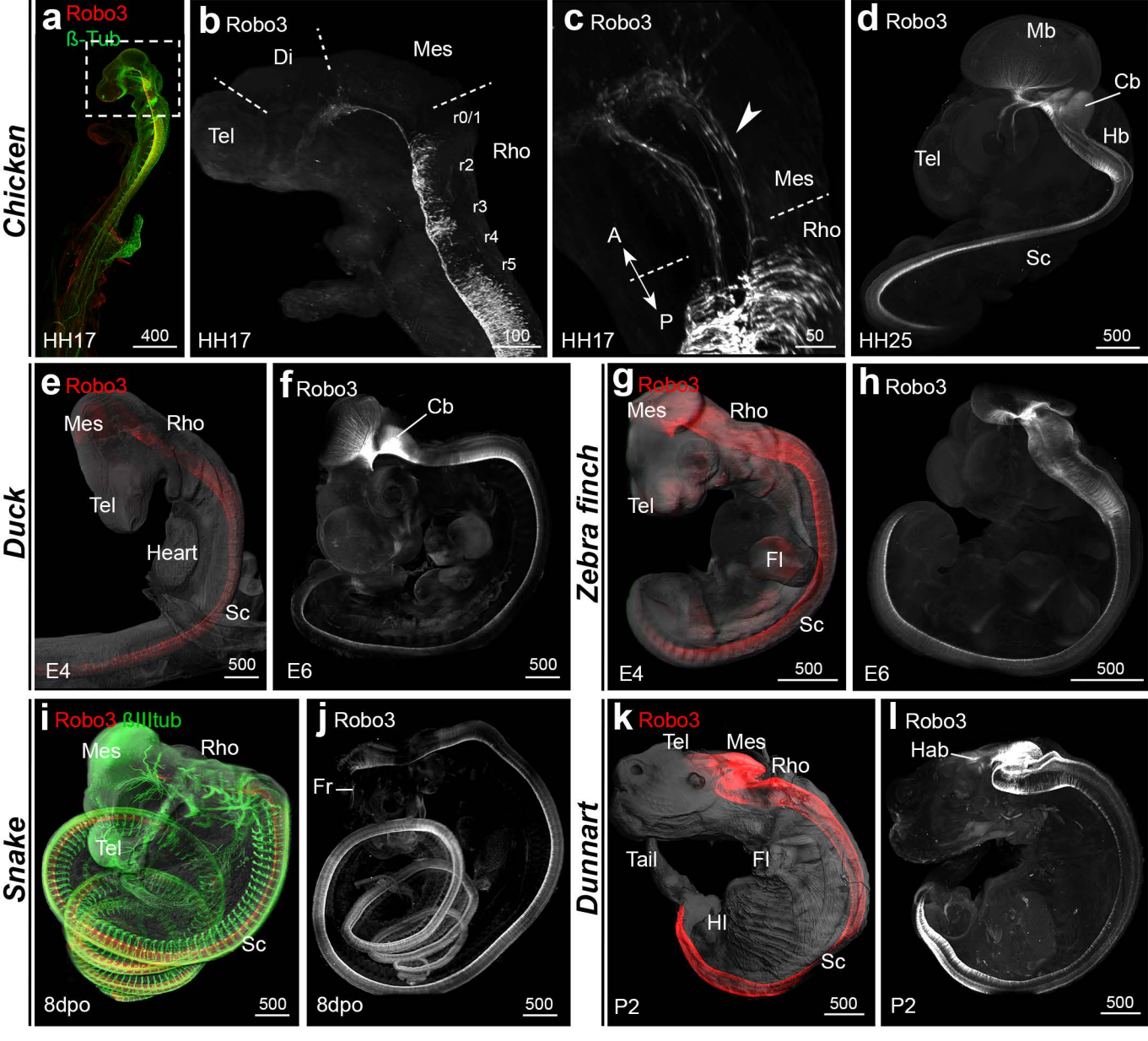
Chicken
a Robo3
ß-Tub
HH17
400
b Robo3
Di
Mes
Tel
r0/1
Rho
r2
r3
r4
r5
HH17
100
c Robo3
Mes
Rho
A
P
HH17
50
d Robo3
Mb
Cb
Hb
Tel
Sc
HH25
500
Duck
e Robo3
Mes
Rho
Tel
Heart
Sc
E4
500
f Robo3
Cb
E6
500
Zebra finch
g Robo3
Mes
Rho
Tel
Fl
Sc
E4
500
h Robo3
E6
500
Snake
i Robo3 ßIIItub
Mes
Rho
Tel
Sc
8dpo
500
j Robo3
Fr
8dpo
500
Dunnart
k Robo3
Tel
Mes
Rho
Tail
Fl
Hl
Sc
P2
500
l Robo3
Hab
P2
500

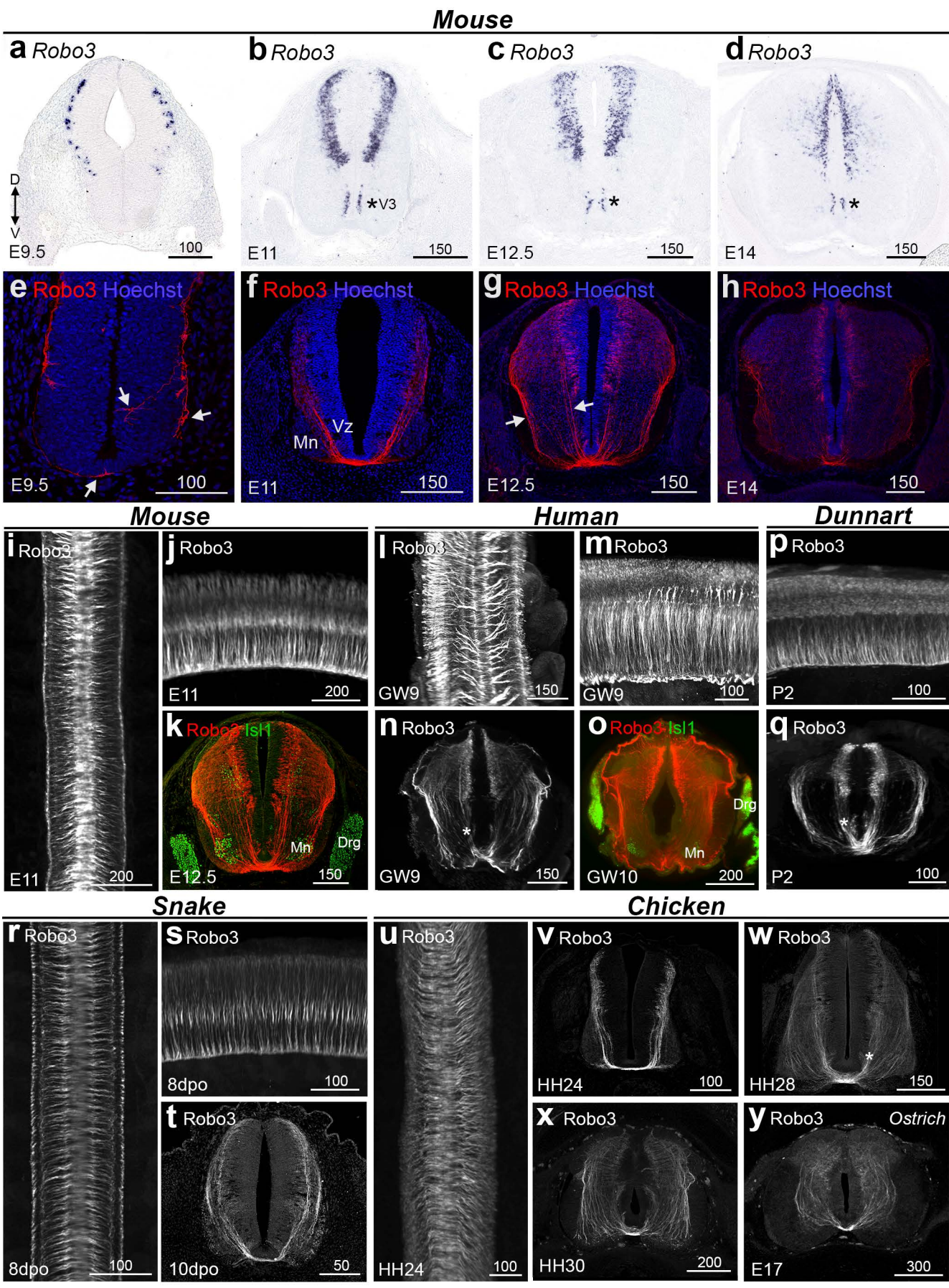
Mouse
a Robo3
D
V
E9.5
100
b Robo3
*V3
E11
150
c Robo3
*
E12.5
150
d Robo3
*
E14
150
e Robo3 Hoechst
E9.5
100
f Robo3 Hoechst
Vz
Mn
E11
150
g Robo3 Hoechst
E12.5
150
h Robo3 Hoechst
E14
150
Mouse
Human
Dunnart
i Robo3
E11
200
j Robo3
E11
200
l Robo3
GW9
150
m Robo3
GW9
100
p Robo3
P2
100
k Robo3 Isl1
Mn
Drg
E12.5
150
n Robo3
*
GW9
150
o Robo3 Isl1
Drg
Mn
GW10
200
q Robo3
*
P2
100
Snake
Chicken
r Robo3
8dpo
100
s Robo3
8dpo
100
t Robo3
10dpo
50
u Robo3
HH24
100
v Robo3
HH24
100
w Robo3
*
HH28
150
x Robo3
HH30
200
y Robo3
Ostrich
E17
300

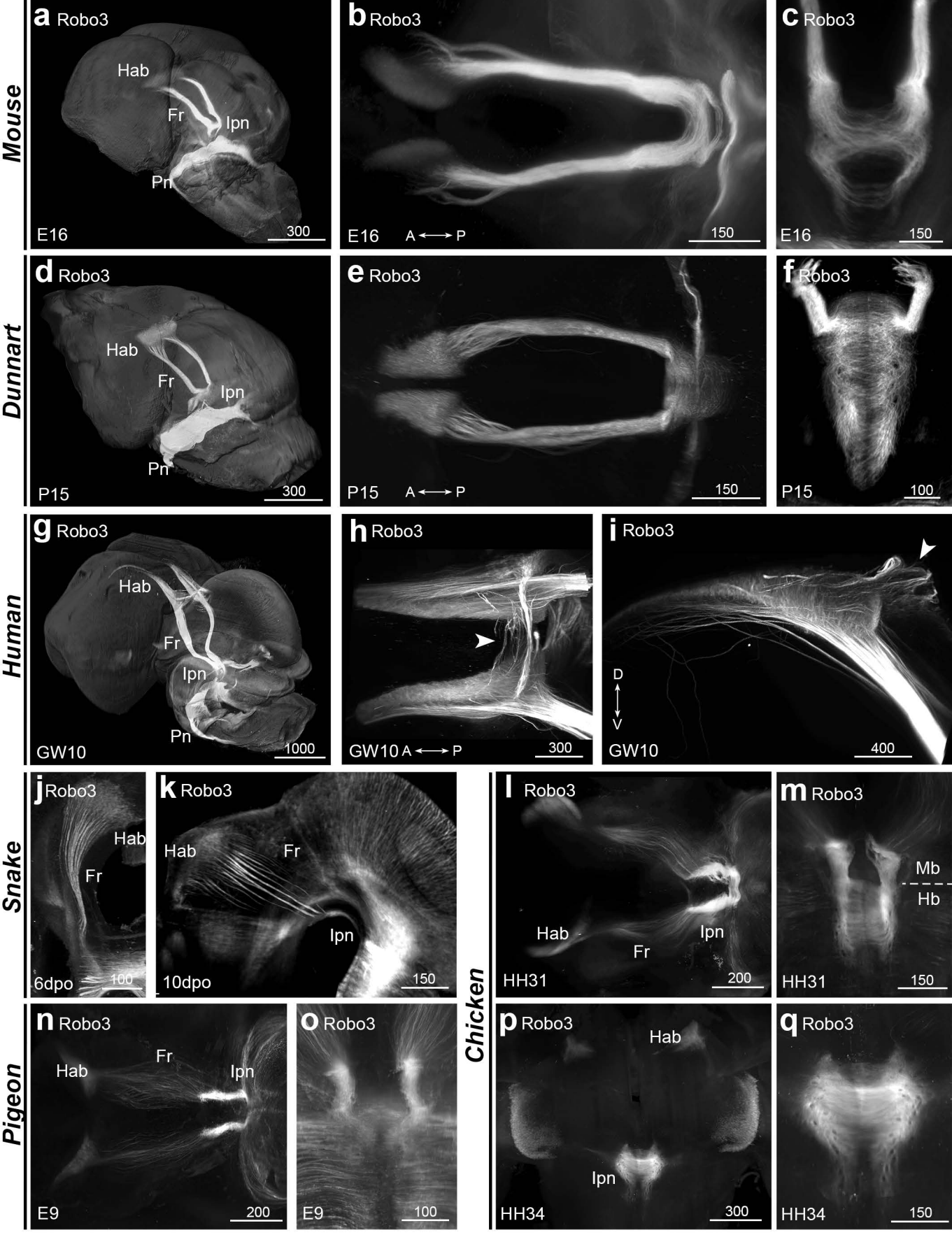
Mouse
a Robo3
Hab
Fr
Ipn
Pn
E16
300
b Robo3
E16
A ⟷ P
150
c Robo3
E16
150
Dunnart
d Robo3
Hab
Fr
Ipn
Pn
P15
300
e Robo3
P15
A ⟷ P
150
f Robo3
P15
100
Human
g Robo3
Hab
Fr
Ipn
Pn
GW10
1000
h Robo3
GW10
A ⟷ P
300
i Robo3
D
V
GW10
400
Snake
j Robo3
Hab
Fr
6dpo
100
k Robo3
Hab
Fr
Ipn
10dpo
150
Chicken
l Robo3
Hab
Fr
Ipn
HH31
200
m Robo3
Mb
Hb
HH31
150
Pigeon
n Robo3
Hab
Fr
Ipn
E9
200
o Robo3
E9
100
p Robo3
Hab
Ipn
HH34
300
q Robo3
HH34
150

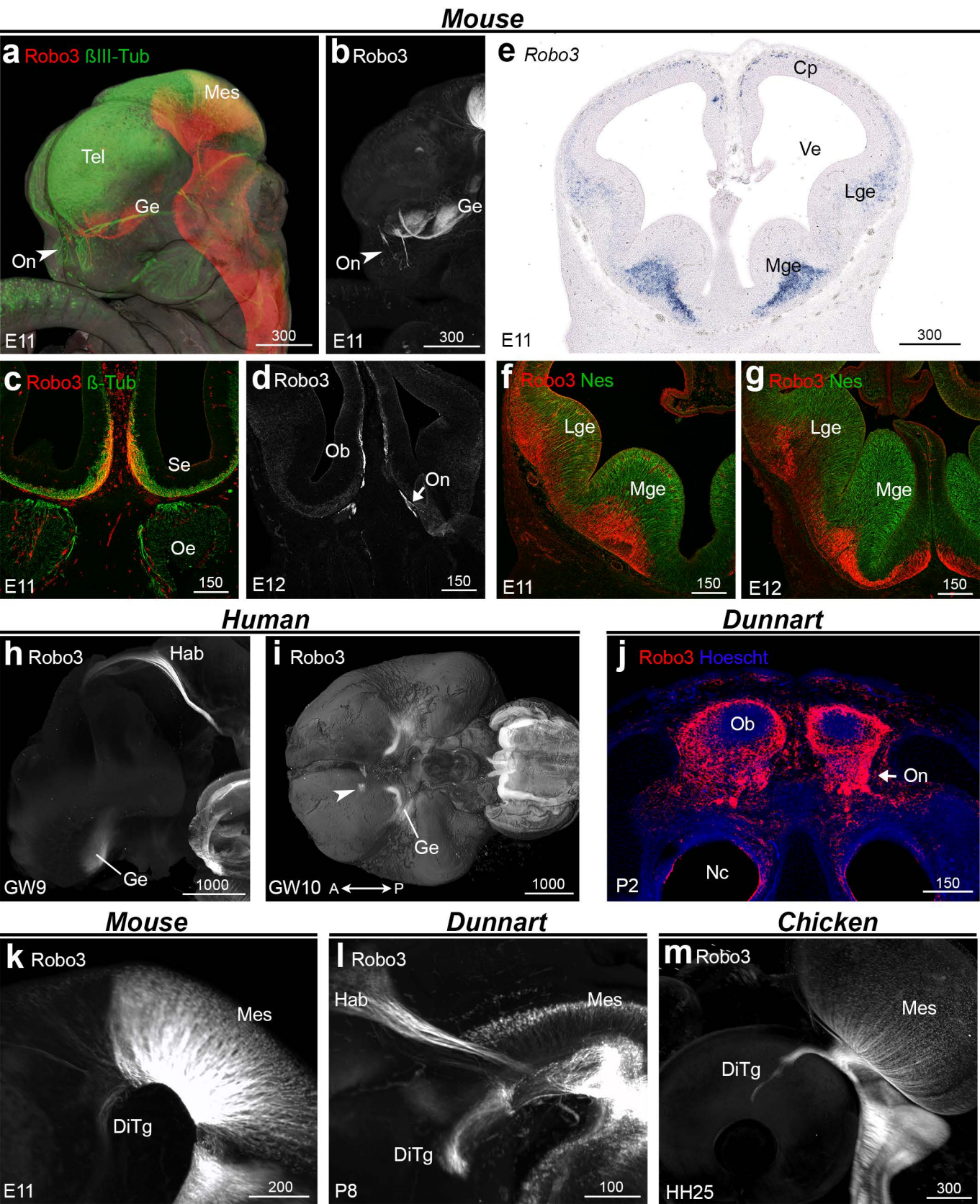
Mouse
a Robo3 ßIII-Tub
Mes
Tel
Ge
On
E11
300
b Robo3
Ge
On
E11
300
e Robo3
Cp
Ve
Lge
Mge
E11
300
c Robo3 ß-Tub
Se
Oe
E11
150
d Robo3
Ob
On
E12
150
f Robo3 Nes
Lge
Mge
E11
150
g Robo3 Nes
Lge
Mge
E12
150
Human
h Robo3
Hab
Ge
GW9
1000
i Robo3
Ge
GW10 A P
1000
Dunnart
j Robo3 Hoescht
Ob
On
Nc
P2
150
Mouse
k Robo3
Mes
DiTg
E11
200
Dunnart
l Robo3
Hab
Mes
DiTg
P8
100
Chicken
m Robo3
Mes
DiTg
HH25
300

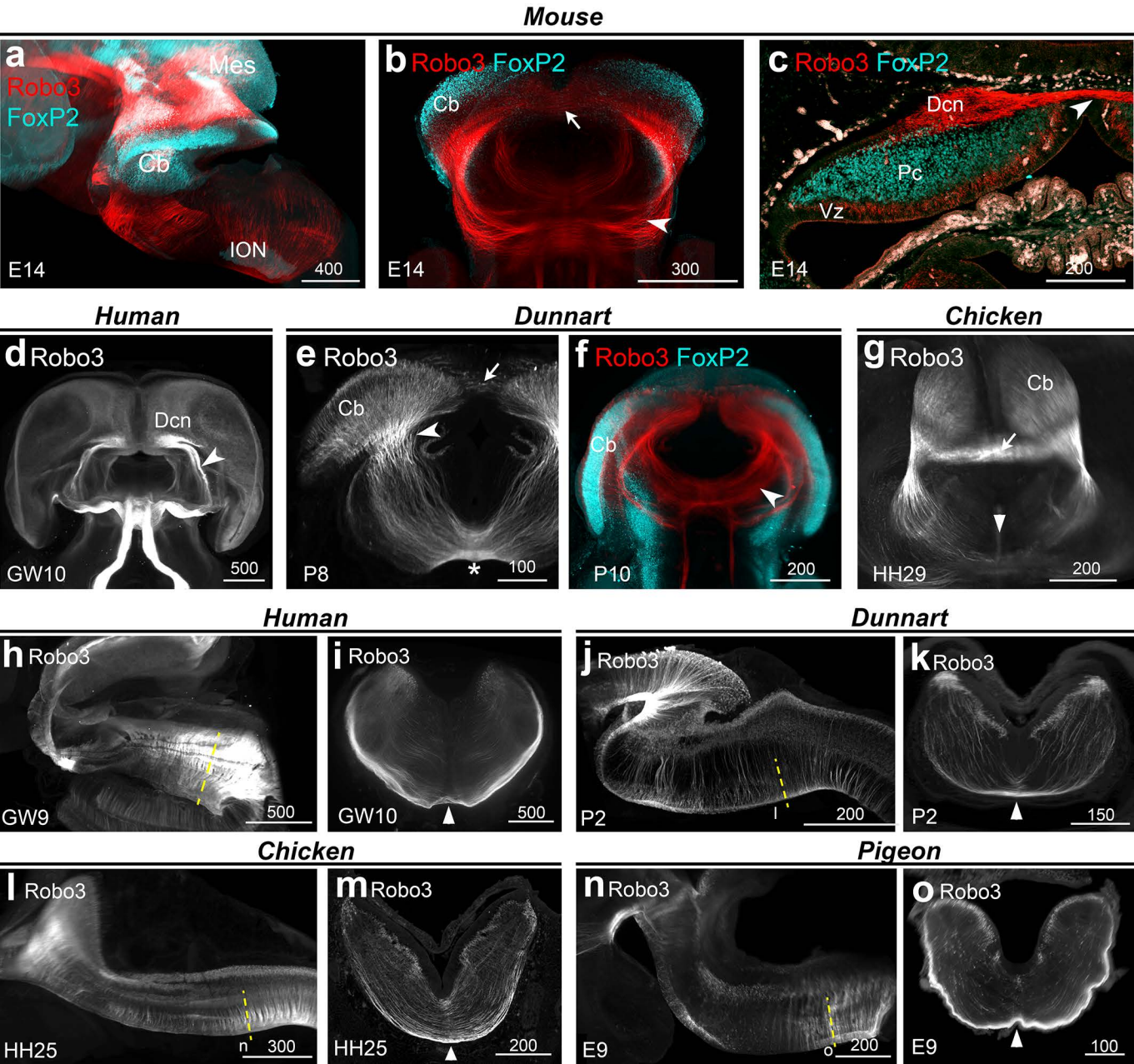
Mouse
a
Robo3
FoxP2
Mes
Cb
ION
E14
400
b Robo3 FoxP2
Cb
E14
300
c Robo3 FoxP2
Dcn
Pc
Vz
E14
200
Human
Dunnart
Chicken
d Robo3
Dcn
GW10
500
e Robo3
Cb
P8
100
f Robo3 FoxP2
Cb
P10
200
g Robo3
Cb
HH29
200
Human
Dunnart
h Robo3
GW9
500
i Robo3
GW10
500
j Robo3
l
P2
200
k Robo3
P2
150
Chicken
Pigeon
l Robo3
n
HH25
300
m Robo3
HH25
200
n Robo3
o
E9
200
o Robo3
E9
100

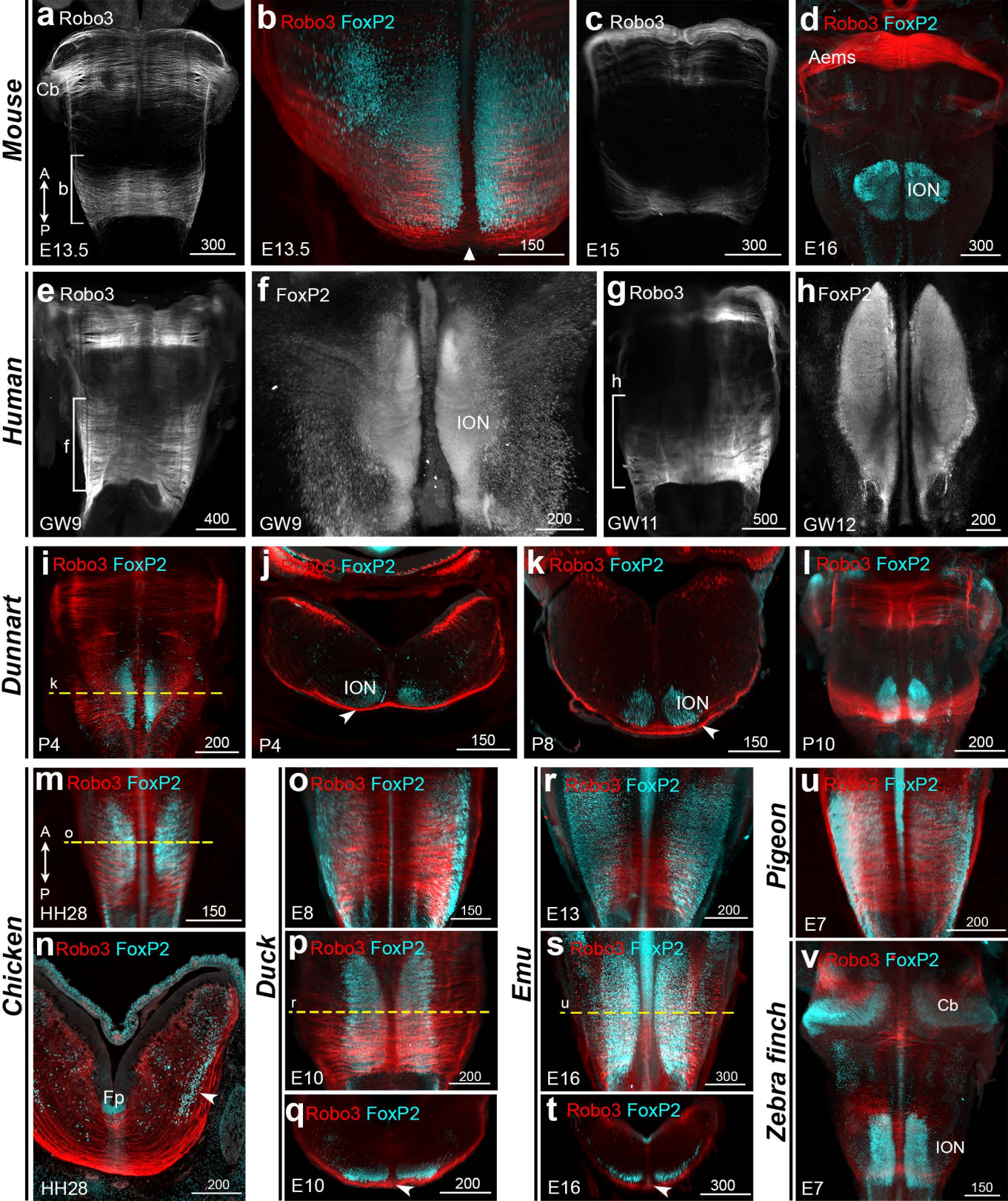
Mouse
a Robo3
Cb
A
b
P
E13.5
300
b Robo3 FoxP2
E13.5
150
c Robo3
E15
300
d Robo3 FoxP2
Aems
ION
E16
300
Human
e Robo3
f
GW9
400
f FoxP2
ION
GW9
200
g Robo3
h
GW11
500
h FoxP2
GW12
200
Dunnart
i Robo3 FoxP2
k
P4
200
j Robo3 FoxP2
ION
P4
150
k Robo3 FoxP2
ION
P8
150
l Robo3 FoxP2
P10
200
Chicken
m Robo3 FoxP2
A
o
P
HH28
150
n Robo3 FoxP2
Fp
HH28
200
Duck
o Robo3 FoxP2
E8
150
p Robo3 FoxP2
r
E10
200
q Robo3 FoxP2
E10
200
Emu
r Robo3 FoxP2
E13
200
s Robo3 FoxP2
u
E16
300
t Robo3 FoxP2
E16
300
Pigeon
u Robo3 FoxP2
E7
200
Zebra finch
v Robo3 FoxP2
Cb
ION
E7
150

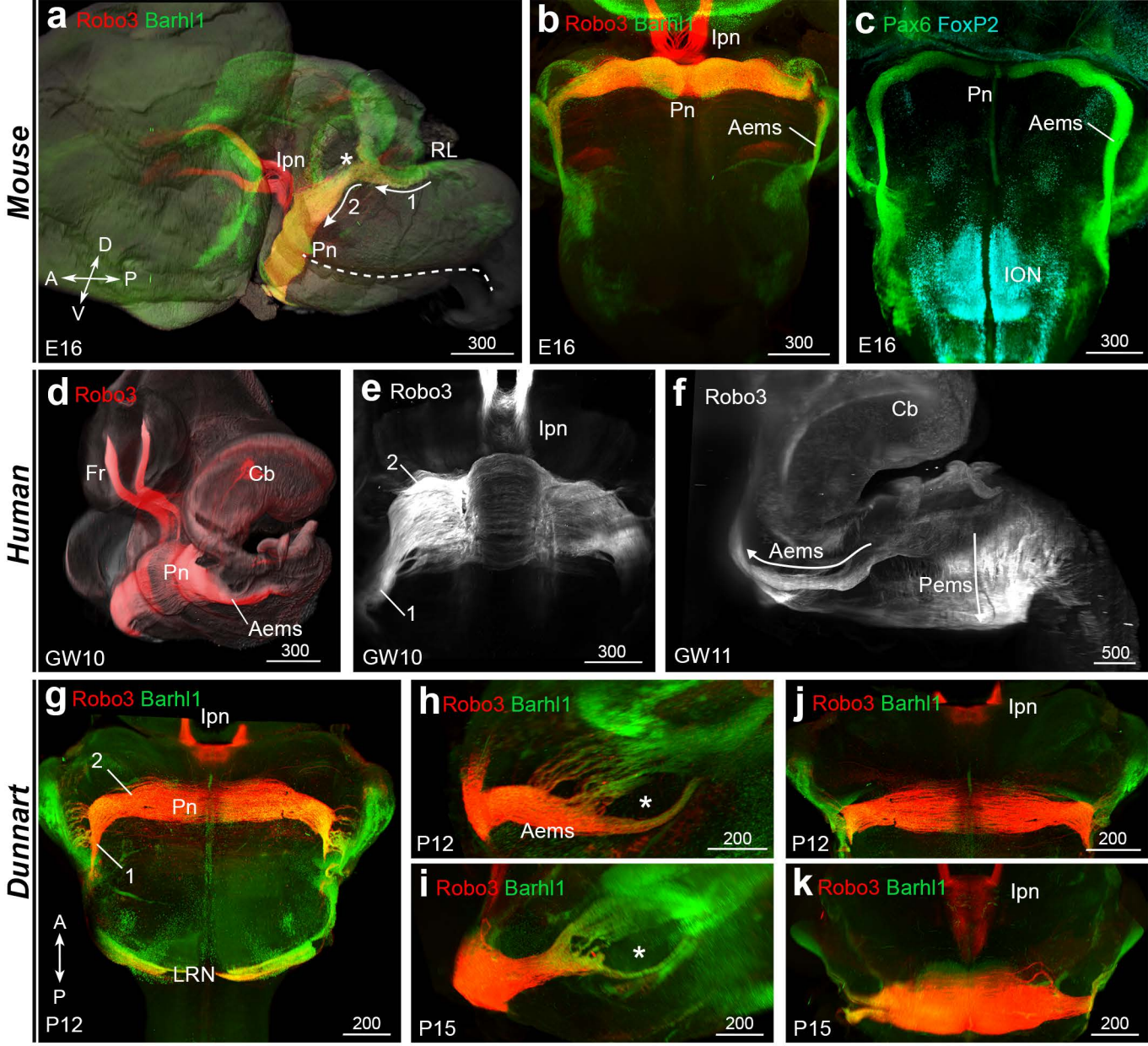
Mouse
Human
Dunnart
a Robo3 Barhl1
Ipn
*
RL
2
1
Pn
D
A
P
V
E16
300
b Robo3 Barhl1
Ipn
Pn
Aems
E16
300
c Pax6 FoxP2
Pn
Aems
ION
E16
300
d Robo3
Fr
Cb
Pn
Aems
GW10
300
e Robo3
Ipn
2
1
GW10
300
f Robo3
Cb
Aems
Pems
GW11
500
g Robo3 Barhl1
Ipn
2
Pn
1
A
P
LRN
P12
200
h Robo3 Barhl1
*
Aems
P12
200
i Robo3 Barhl1
*
P15
200
j Robo3 Barhl1
Ipn
P12
200
k Robo3 Barhl1
Ipn
P15
200

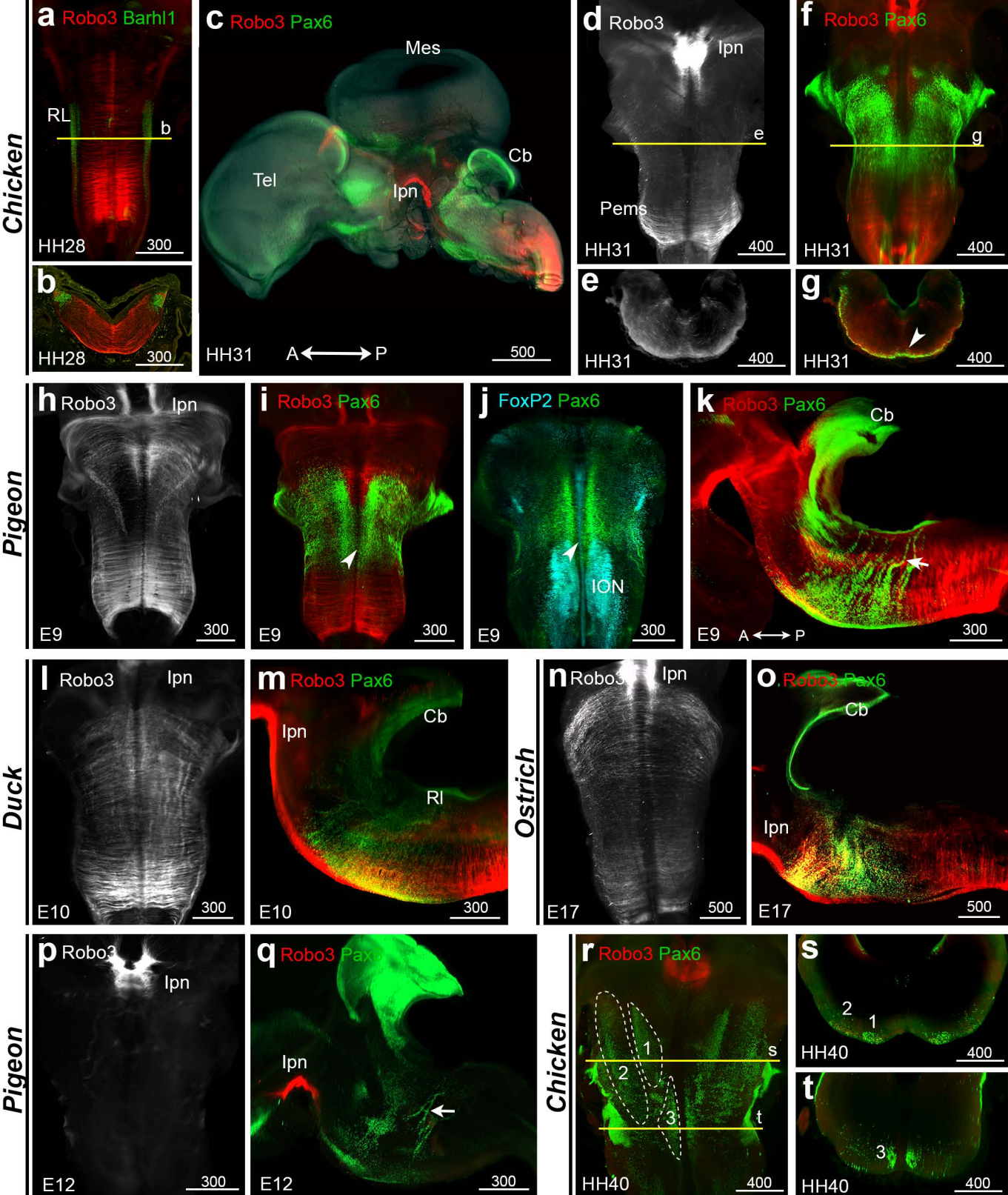
Chicken
a Robo3 Barhl1
RL
b
HH28
300
b
HH28
300
c Robo3 Pax6
Mes
Tel
Cb
Ipn
HH31
A
P
500
d Robo3
Ipn
e
Pems
HH31
400
e
HH31
400
f Robo3 Pax6
g
HH31
400
g
HH31
400
Pigeon
h Robo3
Ipn
E9
300
i Robo3 Pax6
E9
300
j FoxP2 Pax6
ION
E9
300
k Robo3 Pax6
Cb
E9
A
P
300
Duck
l Robo3
Ipn
E10
300
m Robo3 Pax6
Cb
Ipn
Rl
E10
300
Ostrich
n Robo3
Ipn
E17
500
o Robo3 Pax6
Cb
Ipn
E17
500
Pigeon
p Robo3
Ipn
E12
300
q Robo3 Pax6
Ipn
E12
300
Chicken
r Robo3 Pax6
1
2
3
s
t
HH40
400
s
2
1
HH40
400
t
3
HH40
400

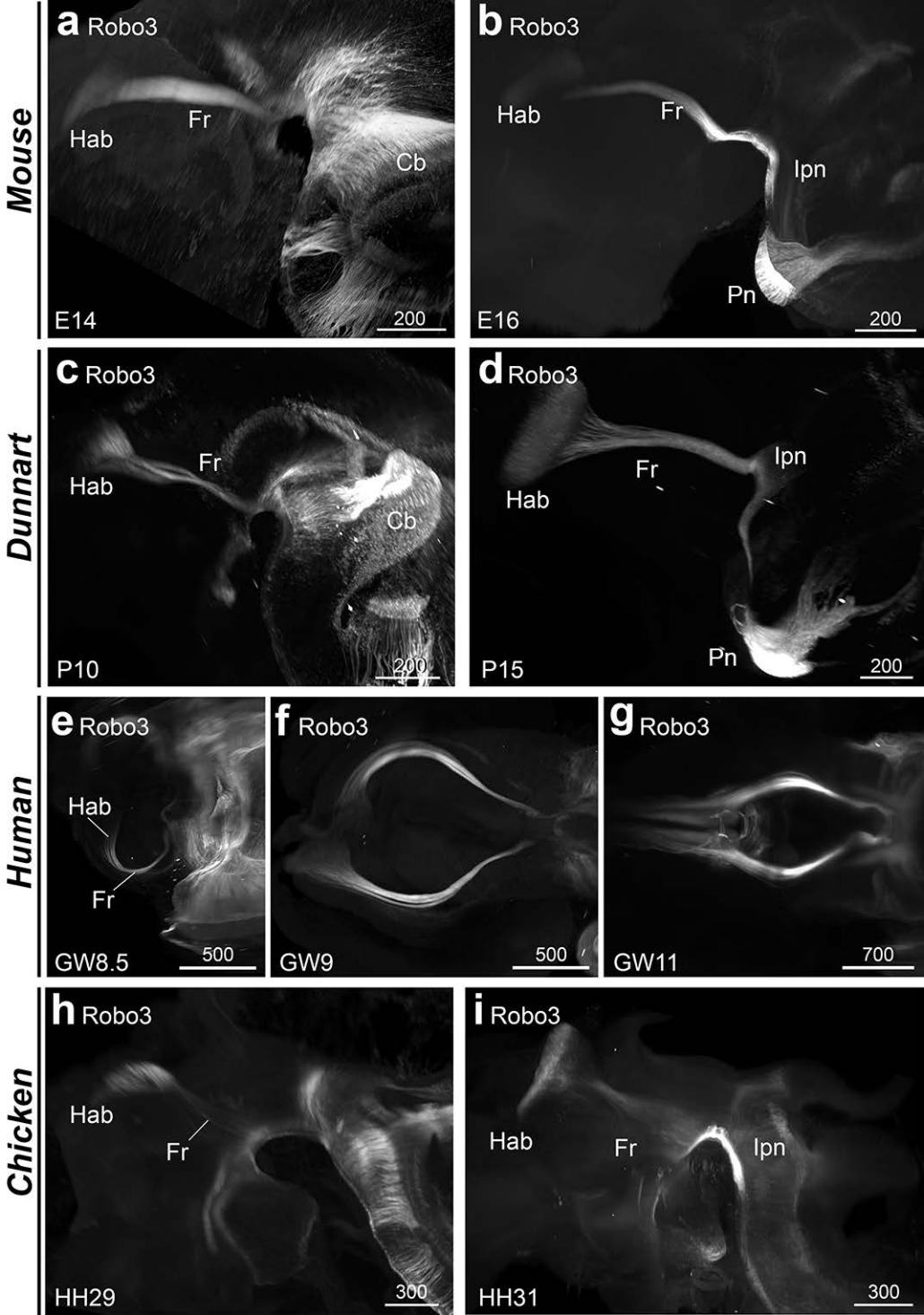
Mouse
a Robo3
Hab
Fr
Cb
E14
200
b Robo3
Hab
Fr
Ipn
Pn
E16
200
Dunnart
c Robo3
Fr
Hab
Cb
P10
200
d Robo3
Ipn
Fr
Hab
Pn
P15
200
Human
e Robo3
Hab
Fr
GW8.5
500
f Robo3
GW9
500
g Robo3
GW11
700
Chicken
h Robo3
Hab
Fr
HH29
300
i Robo3
Hab
Fr
Ipn
HH31
300

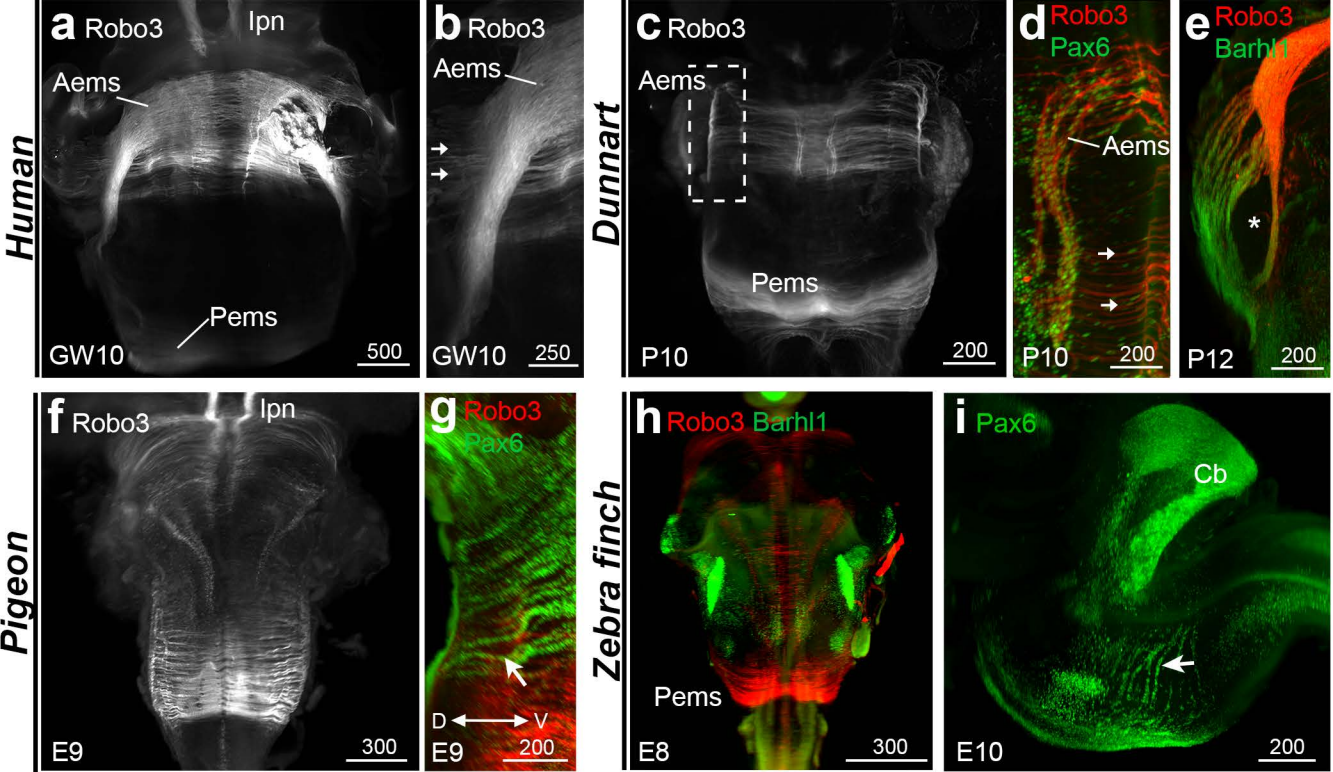
Human
a Robo3
Ipn
Aems
Pems
GW10
500
b Robo3
Aems
GW10
250
Dunnart
c Robo3
Aems
Pems
P10
200
d Robo3
Pax6
Aems
P10
200
e Robo3
Barhl1
*
P12
200
Pigeon
f Robo3
Ipn
E9
300
g Robo3
Pax6
D
V
E9
200
Zebra finch
h Robo3 Barhl1
Pems
E8
300
i Pax6
Cb
E10
200

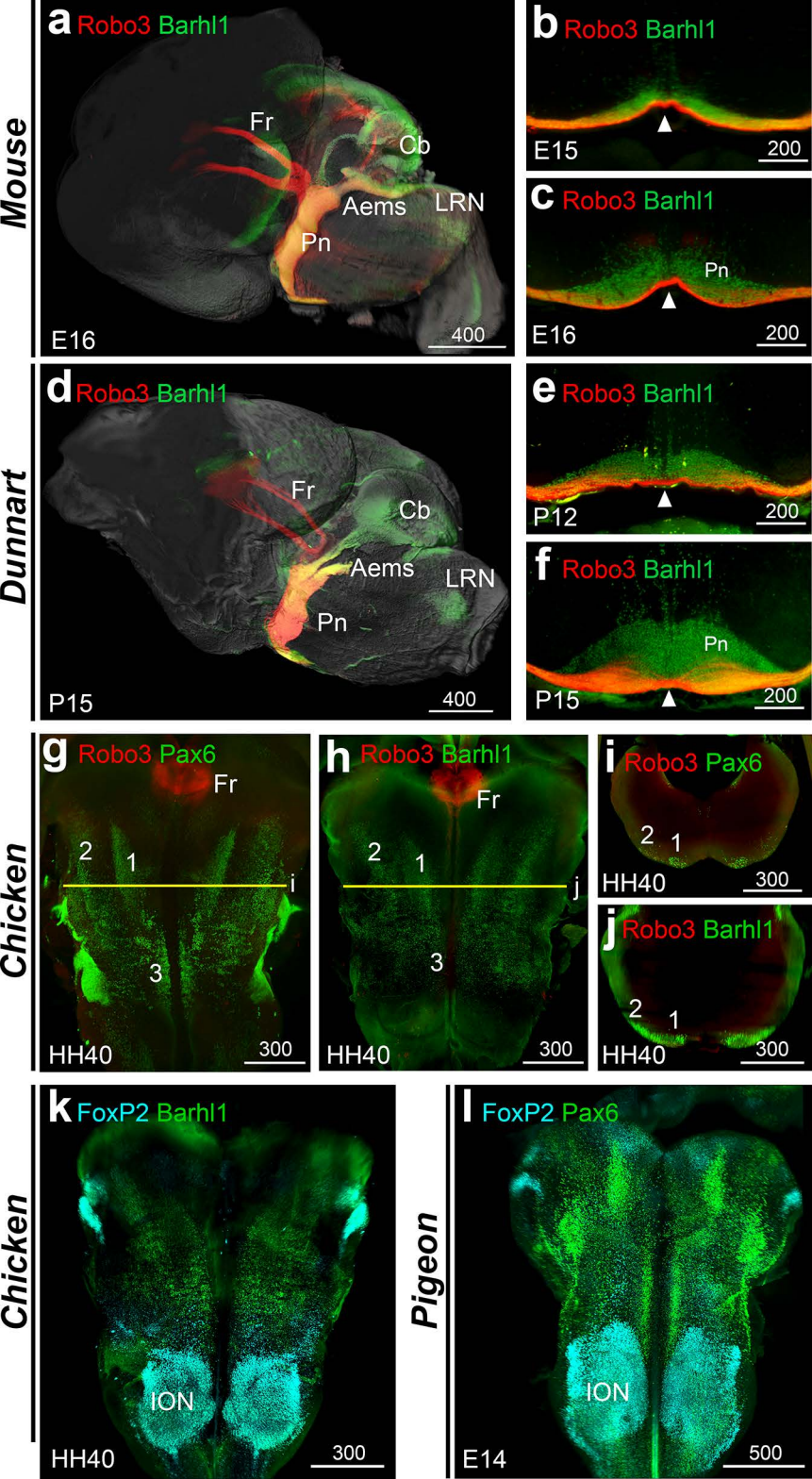
Mouse
a Robo3 Barhl1
Fr
Cb
Aems
LRN
Pn
E16
400
b Robo3 Barhl1
E15
200
c Robo3 Barhl1
Pn
E16
200
Dunnart
d Robo3 Barhl1
Fr
Cb
Aems
LRN
Pn
P15
400
e Robo3 Barhl1
P12
200
f Robo3 Barhl1
Pn
P15
200
Chicken
g Robo3 Pax6
Fr
2
1
i
3
HH40
300
h Robo3 Barhl1
Fr
2
1
j
3
HH40
300
i Robo3 Pax6
2
1
HH40
300
j Robo3 Barhl1
2
1
HH40
300
Chicken
k FoxP2 Barhl1
ION
HH40
300
Pigeon
l FoxP2 Pax6
ION
E14
500

Table 2: Secondary antibodies used in this study

Secondary antibody	Supplier	Catalogue Number	RRID	Titer
AffiniPure Bovine anti-goat IgG (H+L) Cy3	Jackson ImmunoResearch	805-165-180	AB_2340880	1.5µg/ml
Donkey anti-goat IgG (H+L) Alexa Fluor 647	Jackson ImmunoResearch	805-605-180	AB_2340885	1.5µg/ml
AffiniPure Donkey anti-rabbit IgG (H+L) Cy3	Jackson ImmunoResearch	711-165-152	AB_2307443	1.5µg/ml
AffiniPure Donkey anti-rabbit IgG (H+L) Alexa Fluor 647	Jackson ImmunoResearch	711-605-152	AB_2492288	1.5µg/ml